



**NAVAL
POSTGRADUATE
SCHOOL**

MONTEREY, CALIFORNIA

THESIS

**WASTE HEAT RECOVERY CARBON DIOXIDE HEAT
EXCHANGER FOR GAS TURBINE ENGINES**

by

Samuele J. Polsinelli

June 2018

Thesis Advisor:

Garth V. Hobson

Co-Advisor:

Douglas L. Seivwright

Approved for public release. Distribution is unlimited.

THIS PAGE INTENTIONALLY LEFT BLANK

REPORT DOCUMENTATION PAGE			Form Approved OMB No. 0704-0188	
Public reporting burden for this collection of information is estimated to average 1 hour per response, including the time for reviewing instruction, searching existing data sources, gathering and maintaining the data needed, and completing and reviewing the collection of information. Send comments regarding this burden estimate or any other aspect of this collection of information, including suggestions for reducing this burden, to Washington headquarters Services, Directorate for Information Operations and Reports, 1215 Jefferson Davis Highway, Suite 1204, Arlington, VA 22202-4302, and to the Office of Management and Budget, Paperwork Reduction Project (0704-0188) Washington, DC 20503.				
1. AGENCY USE ONLY (Leave blank)		2. REPORT DATE June 2018	3. REPORT TYPE AND DATES COVERED Master's thesis	
4. TITLE AND SUBTITLE WASTE HEAT RECOVERY CARBON DIOXIDE HEAT EXCHANGER FOR GAS TURBINE ENGINES			5. FUNDING NUMBERS ONR ESTEP	
6. AUTHOR(S) Samuele J. Polsinelli				
7. PERFORMING ORGANIZATION NAME(S) AND ADDRESS(ES) Naval Postgraduate School Monterey, CA 93943-5000			8. PERFORMING ORGANIZATION REPORT NUMBER	
9. SPONSORING / MONITORING AGENCY NAME(S) AND ADDRESS(ES) N/A			10. SPONSORING / MONITORING AGENCY REPORT NUMBER	
11. SUPPLEMENTARY NOTES The views expressed in this thesis are those of the author and do not reflect the official policy or position of the Department of Defense or the U.S. Government.				
12a. DISTRIBUTION / AVAILABILITY STATEMENT Approved for public release. Distribution is unlimited.			12b. DISTRIBUTION CODE A	
13. ABSTRACT (maximum 200 words) The U.S. Navy is looking to conserve energy on shore and at sea. As a contribution to the ongoing effort to make turbine engines more efficient, this research presents the design and analysis of a helical coil waste heat recovery heat exchanger for a Rolls Royce T63-A-720 gas turbine engine. The T-63 engine was installed in the test cell and modified, with the appropriate instrumentation added. The waste heat recovery heat exchanger was designed for a future closed Brayton cycle loop. Analysis was conducted on the heat exchanger's effect on the engine backpressure, which was shown to be negligible. Further analysis showed the heat exchanger was capable of meeting the requirements laid out by NPS student Aaron VanDenBerg in his 2016 thesis, "Energy Efficient Waste Heat Recovery From an Engine Exhaust System." Finally, a study varying the pressure drop through the heat exchanger was conducted and a projected performance curve of the heat exchanger was developed. An analytical equation was derived determining the mass flow for a required exit temperature. Our research findings indicate promise for waste heat recovery using a helical coil heat exchanger. We recommend building and testing the heat exchanger to verify the model.				
14. SUBJECT TERMS heat exchanger, CFD, CFX, T-63 installation, helical coil heat exchanger, waste heat recovery, carbon dioxide CO2, cogeneration, gas turbine engine instrumentation			15. NUMBER OF PAGES 81	
			16. PRICE CODE	
17. SECURITY CLASSIFICATION OF REPORT Unclassified	18. SECURITY CLASSIFICATION OF THIS PAGE Unclassified	19. SECURITY CLASSIFICATION OF ABSTRACT Unclassified	20. LIMITATION OF ABSTRACT UU	

THIS PAGE INTENTIONALLY LEFT BLANK

Approved for public release. Distribution is unlimited.

**WASTE HEAT RECOVERY CARBON DIOXIDE HEAT EXCHANGER FOR
GAS TURBINE ENGINES**

Samuele J. Polsinelli
Ensign, United States Navy
BS, U.S. Naval Academy, 2017

Submitted in partial fulfillment of the
requirements for the degree of

MASTER OF SCIENCE IN MECHANICAL ENGINEERING

from the

**NAVAL POSTGRADUATE SCHOOL
June 2018**

Approved by: Garth V. Hobson
Advisor

Douglas L. Seivwright
Co-Advisor

Garth V. Hobson
Chair, Department of Mechanical and Aerospace Engineering

THIS PAGE INTENTIONALLY LEFT BLANK

ABSTRACT

The U.S. Navy is looking to conserve energy on shore and at sea. As a contribution to the ongoing effort to make turbine engines more efficient, this research presents the design and analysis of a helical coil waste heat recovery heat exchanger for a Rolls Royce T63-A-720 gas turbine engine. The T-63 engine was installed in the test cell and modified, with the appropriate instrumentation added. The waste heat recovery heat exchanger was designed for a future closed Brayton cycle loop. Analysis was conducted on the heat exchanger's effect on the engine backpressure, which was shown to be negligible. Further analysis showed the heat exchanger was capable of meeting the requirements laid out by NPS student Aaron VanDenBerg in his 2016 thesis, "Energy Efficient Waste Heat Recovery from an Engine Exhaust System." Finally, a study varying the pressure drop through the heat exchanger was conducted and a projected performance curve of the heat exchanger was developed. An analytical equation was derived determining the mass flow for a required exit temperature. Our research findings indicate promise for waste heat recovery using a helical coil heat exchanger. We recommend building and testing the heat exchanger to verify the model.

THIS PAGE INTENTIONALLY LEFT BLANK

TABLE OF CONTENTS

I.	INTRODUCTION.....	1
A.	MOTIVATION	1
B.	BACKGROUND	1
1.	Gas Turbines and the Brayton Cycle	1
2.	Cogeneration Plants and Waste Heat Recovery	1
3.	Working Fluid Selection.....	2
C.	OBJECTIVE	2
II.	ENGINE INSTALLATION AND BASELINE	5
A.	INTRODUCTION.....	5
B.	INDICATION OF DRIVE SHAFT.....	5
C.	ENGINE INSTALLATION AND BRACING.....	6
D.	ENGINE ALIGNMENT.....	7
E.	AIR INTAKE DESIGN	7
1.	Bell Mouth Design.....	8
2.	Flange.....	9
III.	DUCT AND HEAT EXCHANGER DESIGN.....	11
A.	DUCT DESIGN.....	11
B.	PRELIMINARY DESIGN CALCULATIONS.....	14
1.	Heat Transfer	14
2.	Compressibility Limits	14
C.	HEAT EXCHANGER DESIGN.....	15
D.	MANIFOLD	17
IV.	CFD MODELING, PREDICTIONS, AND PERFORMANCE.....	19
A.	INTRODUCTION.....	19
B.	BACKPRESSURE MOLDING	19
1.	SolidWorks Model	19
2.	Meshing.....	20
3.	Setup.....	22
4.	Results	22
C.	COUPLED HEAT TRANSFER MODEL	23
1.	Mass Flow Driven Model	23
2.	Steady State Pressure Driven Boundary Conditions.....	29
3.	Pressure Driven Transient Results.....	31
4.	Pressure Driven Transient Analytical Solution	32

5.	Heat Transfer and Flow Segregation	34
6.	Mesh Independence	37
V.	CONCLUSION AND RECOMMENDATIONS FOR FUTURE WORK.....	39
A.	CONCLUSION	39
B.	FUTURE WORK.....	39
	APPENDIX A. HEAT EXCHANGER HAND CALCULATIONS.....	41
	APPENDIX B. LINE DIAGRAM FOR MANIFOLD.....	43
	APPENDIX C. REFERENCE LINE LOCATIONS.....	45
	APPENDIX D. ISOTHERMAL VELOCITY AND PRESSURE.....	47
	APPENDIX E. HEAT TRANSFER VELOCITY AND PRESSURE DISTRIBUTION.....	49
	APPENDIX F. FULL PRESSURE STUDY RESULTS	51
	APPENDIX G. RESTARTING A RUN ON HAMMING.....	59
	LIST OF REFERENCES	61
	INITIAL DISTRIBUTION LIST	63

LIST OF FIGURES

Figure 1	Waste Heat Recovery System Schematic	3
Figure 2	Schematic of the T63-A-720 Engine	5
Figure 3	Drive Shaft Indication Diagram.....	6
Figure 4	Schematic Drawing of Air Intake System	7
Figure 5	Bell Mouth SolidWorks Model.....	8
Figure 6	Bell Mouth Installed on Engine	9
Figure 7	Flange Model Cross Section	10
Figure 8	Exhaust Ducts by VanDenBerg. Source: [1].	11
Figure 9	Assembled Model of Duct with Heat Exchanger Coils	12
Figure 10	Installed Heat Exchanger Duct	13
Figure 11	Axial View of Heat Exchanger	16
Figure 12	Flow Volume for Backpressure Model.....	20
Figure 13	Backpressure Mesh 2	21
Figure 14	Backpressure Mesh 5	21
Figure 15	Backpressure Results (make them the same size).....	22
Figure 16	Swirl Induced in the Flow.....	23
Figure 17	Mesh Overview for Coupled Mesh.....	25
Figure 18	Detail of Mesh 4.....	25
Figure 19	Detail of Mesh 4 Inflation Layer	26
Figure 20	Heat Transfer Convergence History in Exhaust Flow	27
Figure 21	Mass Flow Driven CFD Results	28
Figure 22	Mass Flow Driven Tube Temperatures.....	29
Figure 23	Streamline in a Vortex	32

Figure 24	Transient Pressure Study Results.....	33
Figure 25	Tube Temperatures for Pressure Driven Boundry Conditions	35
Figure 26	Heat Transfer Coefficient on Bottom of Coils.....	36
Figure 27	Streamline Visualization, Colored for Temperature.....	37

LIST OF TABLES

Table 1.	Drive Shaft Runout by Location	6
Table 2.	Coil Length Calculations	14
Table 3.	Backpressure Mesh Summary.....	20
Table 4.	Backpressure Results Summary.....	23
Table 5.	Coupled Model Mesh Metrics	24
Table 6.	Mass Flow Driven Heat Transfer CFD Results	28
Table 7.	Transient and Steady State Comparison	31

THIS PAGE INTENTIONALLY LEFT BLANK

LIST OF ACRONYMS AND ABBREVIATIONS

CFD	Computational Fluid Dynamics
CFX	CFD Software produced by ANSYS corp.
CO ₂	Carbon Dioxide
DoD	Department of Defense
K	Degrees Kelvin
US	United States

THIS PAGE INTENTIONALLY LEFT BLANK

ACKNOWLEDGMENTS

I would like to thank my advisors, Dr. Hobson and Dr. Seivwright, for their support. To Krista, for all of your help this year.

THIS PAGE INTENTIONALLY LEFT BLANK

I. INTRODUCTION

A. MOTIVATION

It is beneficial for the U.S. Navy to conserve energy. As the second-largest consumer of energy in the DoD, reduction in Navy consumption would further the reduction of carbon dioxide in the atmosphere, aid strategic independence and reduce U.S. dependence on oil [1]. The Naval Postgraduate School was tasked by the Office of Naval Research Energy System Evaluation Program with improving the efficiency of gas turbine engines by recovering waste heat from gas turbine exhaust systems.

B. BACKGROUND

1. Gas Turbines and the Brayton Cycle

Gas turbine power plants are employed on U.S. Navy ships because they have a high power to weight ratio [2]. These power plants allow for high speeds and relatively efficient performance. A gas turbine is thermodynamically modeled by the Brayton cycle. The ideal Brayton cycle is isentropic compression, isobaric heating and isentropic expansion [2]. Most Brayton cycles are considered open cycles, where air from the surroundings is used as the working fluid, and heat is rejected from the engine through exhausting the working fluid. A closed Brayton cycle utilizes a second heat exchanger to reject the heat and reuse the same working fluid [2].

2. Cogeneration Plants and Waste Heat Recovery

Open Brayton cycles reject air at high temperatures and atmospheric pressures. It is attractive to recover and reuse some of the waste heat. Currently, this is done in cogeneration plants producing electrical power. Cogeneration plants use the hot exhaust gases to produce steam, which is then used to run a turbine. The recovery of waste heat increases the efficiency of the power plant to above 60%. Many civilian cargo ships utilize waste heat recovery units to increase their efficiency as well. Both cogeneration plants and cargo ships have room for the large equipment required for waste heat recovery.

The U.S. Navy attempted to replicate the land-based, Rankine cogeneration system with boilers installed on the Ticonderoga class cruisers. However, the system installed was inefficient and difficult to maintain [1]. Unlike civilian cargo ships, naval vessels rarely operate at constant speed, increasing the wear on and decreasing the usefulness of the recovery system. After several years, primarily due to corrosion, the heat recovery units became inoperable and were removed from the ships [1].

3. Working Fluid Selection

Carbon dioxide was chosen as the working fluid for a closed Brayton cycle by VanDenBerg in his thesis [1]. VanDenBerg was responsible for the initial work done on this project. Carbon dioxide was chosen as the working fluid for a closed Brayton cycle due to its non-corrosive nature, gaseous operation, and efficiency. The Brayton cycle was chosen over a more efficient transcritical cycle because of the lower operating pressures allowing for ease of construction and use. In these operating conditions, the Brayton cycle is more efficient than the equivalent Rankine cycle, based on thermodynamic analysis and the specific work done in [1]. The low-pressure Brayton cycle is cheaper to produce as specialty materials do not need to be selected, and safety precautions can be lower. Finally, the low pressure system can be pressurized from commercial compressed gas cylinders. Further details and rationale for the selection of a low pressure Brayton cycle can be found in VanDenBerg's thesis [1].

C. OBJECTIVE

The objective of this thesis is to design, build, and test a helical coil waste heat recovery heat exchanger for a Rolls Royce T63-A-720 gas turbine engine. The heat exchanger should not impact the performance of the engine (by inducing backpressure on the engine) and extract as much energy from the exhaust as possible and transfer it to carbon dioxide. Eventually, this carbon dioxide will be used to run a second closed-loop Brayton cycle waste heat recovery system, as shown in Figure 1. The final system will be used for return-on-investment (ROI) studies when complete.

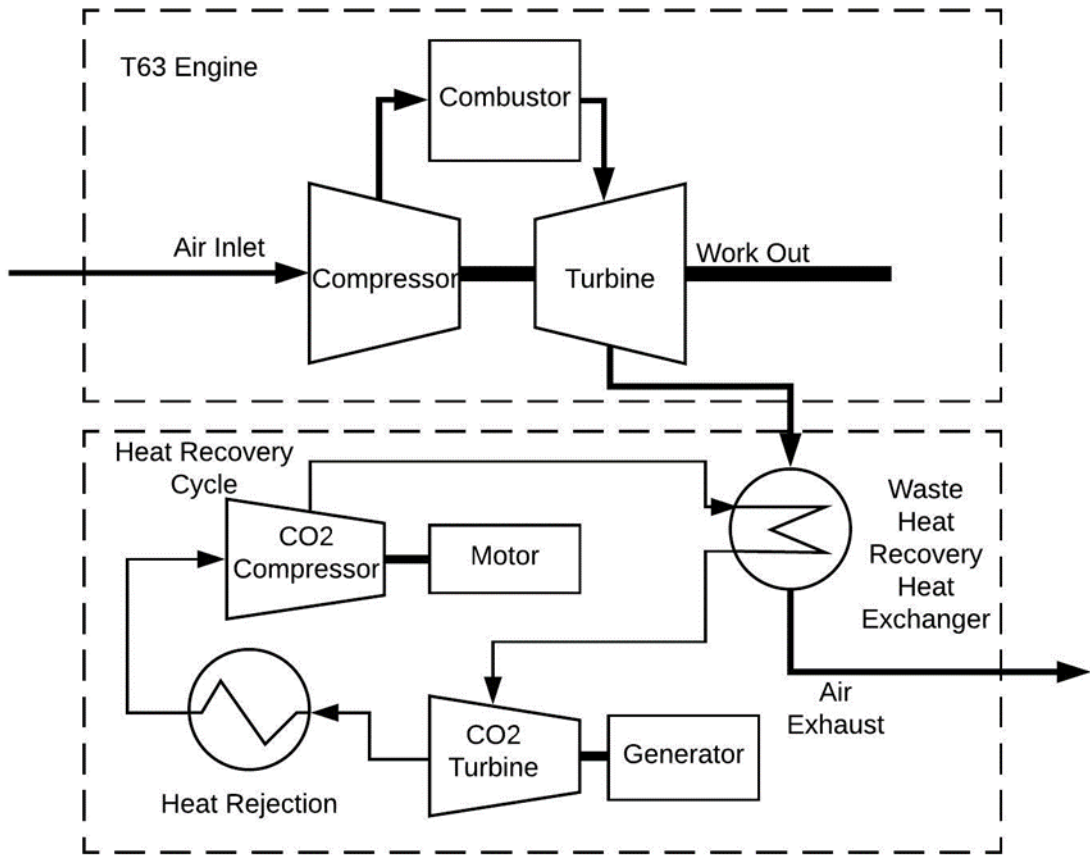


Figure 1. Waste Heat Recovery System Schematic

THIS PAGE INTENTIONALLY LEFT BLANK

II. ENGINE INSTALLATION AND BASELINE

A. INTRODUCTION

Prior to investigating the viability of a carbon dioxide heat exchanger, an engine had to be acquired and installed. A zero-hour Rolls Royce T63-A-720 engine depicted in Figure 2, was acquired and installed in the Marine Propulsion Laboratory Gas turbine test cell. The engine installation required 0.254mm (0.010 in.) tolerances with dynamometer alignment. The air intake for the engine had to be modified, instrumented and installed as the T63-A-720 was larger than the previous T63-A-700.

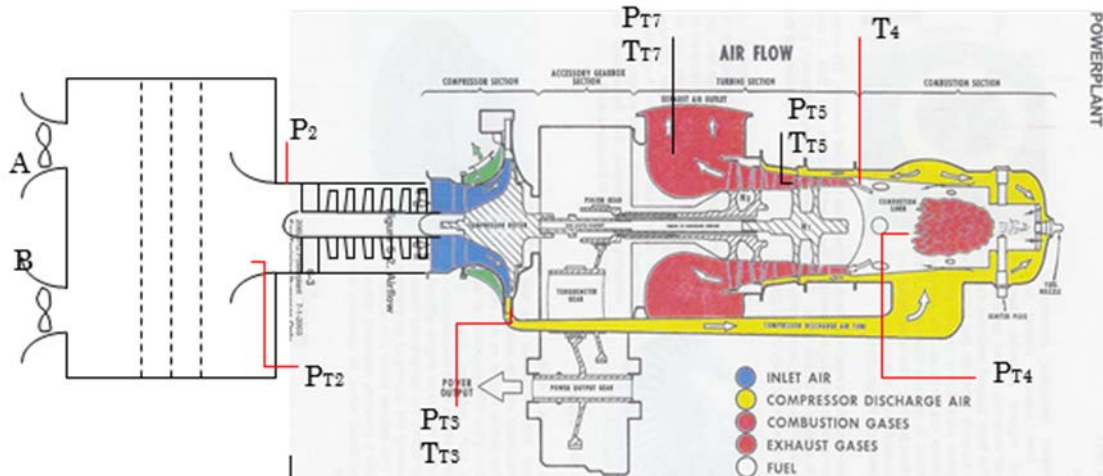


Figure 2. Schematic of the T63-A-720 Engine¹

B. INDICATION OF DRIVE SHAFT

The engine drive shaft was disconnected from the original engine for installation on the new engine. Its spline was checked for compatibility with the new engine. To ensure the drive shaft was not damaged, it was brought to the NPS machine shop for indication on a lathe. The drive shaft was centered in the lathe by the flange and a live center was placed

¹ Figure taken from unpublished ME3240 laboratory handout written by Garth Hobson for the Naval Postgraduate School Monterey CA, in 2013.

at the spline end of the shaft. Because the center of the flange could not be accessed, the spline center was considered to be true.

The shaft was centered and indicated in four separate locations, shown in Figure 3, the flange, flange end of the shaft, center of the shaft and the far, and spline end of the shaft. The measurements, summarized in Table 1, and the runout of 0.0254 mm (0.001 in.) was well within tolerance. The largest runout was on the flange itself, in the chuck. However, the runout was only 0.127 mm (0.005 in.). The measurements indicated that the shaft was not bent, twisted, or bowed. The shaft could safely be used in the new engine without fear of damaging the engine.

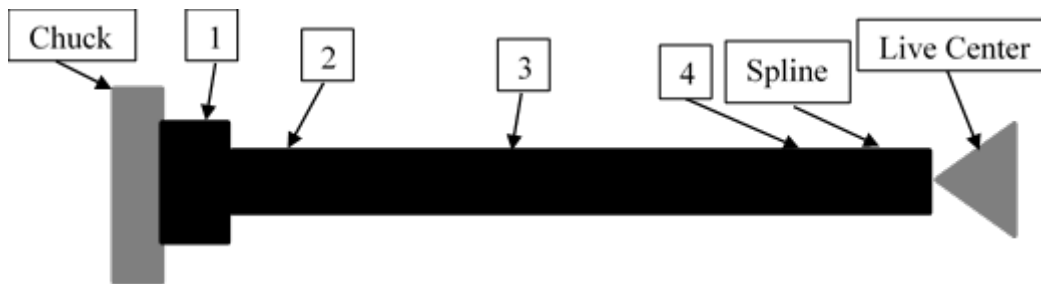


Figure 3. Drive Shaft Indication Diagram

Table 1. Drive Shaft Runout by Location

Location	1	2	3	4
Total Indicated runout mm (in)	0.127 (0.005)	0.0762 (0.003)	0.0508 (0.002)	0.0254 (0.001)

C. ENGINE INSTALLATION AND BRACING

The engine was installed using a hydraulic lift. It was secured to the frame using the existing mounting hardware. During installation, the engine was found to be heavily supported by the air intake described in Section E of this chapter. The air intake, made primarily of Plexiglas, was torquing the engine mount, causing stress, and absorbing

vibrations during operation. Therefore, it was deemed necessary to brace the engine and prevent the air intake from bearing any load.

D. ENGINE ALIGNMENT

The engine was aligned by first removing all of the bolts securing the engine to the test stand. The engine was slid forward to allow installation of the engine drive shaft. Reinstalling the four bolts closest to the inlet plenum aligned the engine left to right. The engine was then shimmed vertically into position with the dynamometer. The shims inserted were 2.54 mm (0.10 in.) thick. Finally, a shim was added under the rear strut to prevent them from twisting the engine mount.

E. AIR INTAKE DESIGN

The air intake system is important for experimental repeatability. The system, shown in Figure 4, includes two flow meters, several screens, and a bell mouth. The screens are important to disperse the jets created by the mass flow meters as well as to straighten the flow entering the bell mouth, which is the final stage before entering the engine compressor. The bell mouth is instrumented for static pressure, total pressure, and temperature. During this thesis, a new bell mouth was designed and manufactured by 3D printing, and a new flange connecting the air intake to the engine was also designed and fabricated.

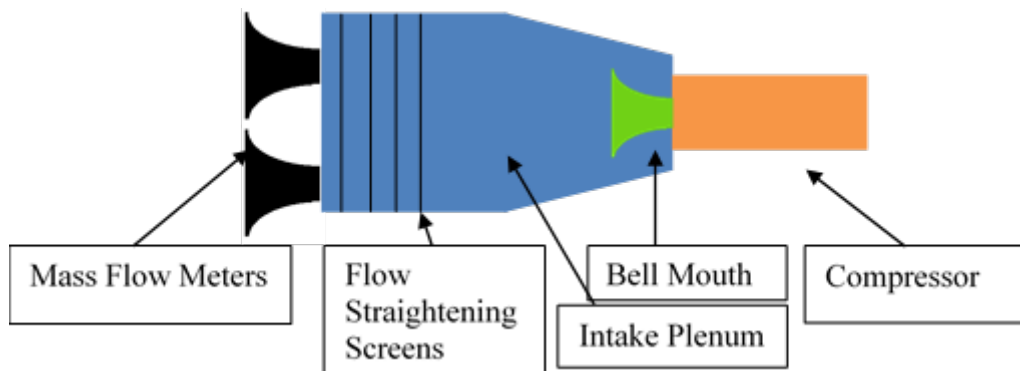


Figure 4. Schematic Drawing of Air Intake System

1. Bell Mouth Design

The bell mouth was designed using an ellipse with a 2:1 ratio based on the diameter of the engine intake. A quarter of the ellipse was revolved to generate the bell mouth. This was revolved around a central axis to form the axi-symmetric shape. The base was thickened to allow support for the bolts holding the bell mouth in place, and the probe mounted to the bell mouth. A SolidWorks model of the bell mouth is shown in Figure 5.

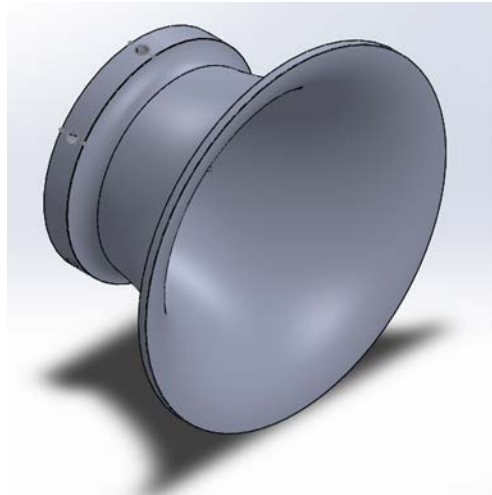


Figure 5. Bell Mouth SolidWorks Model

The bell mouth was 3D printed using polycarbonate for ease of manufacture, which took 24 hours to produce. The bell mouth was then tapped and inserts added for support. The instruments were directly tapped into the side of the bell housing. It was assumed that they would not need to be removed or replaced often and there was little weight being supported. Therefore, it was unnecessary to reinforce the connections, and a direct tap to the plastic would suffice.

The bell mouth was instrumented with three static pressure ports, two thermocouples, and a stagnation pressure probe. The static pressure ports required three holes 0.794mm (0.03125 in.) in diameter. The probes and thermocouples were 3.175mm (1/8th in.). All were secured using Teflon sealant. The final installation can be seen in Figure 6.

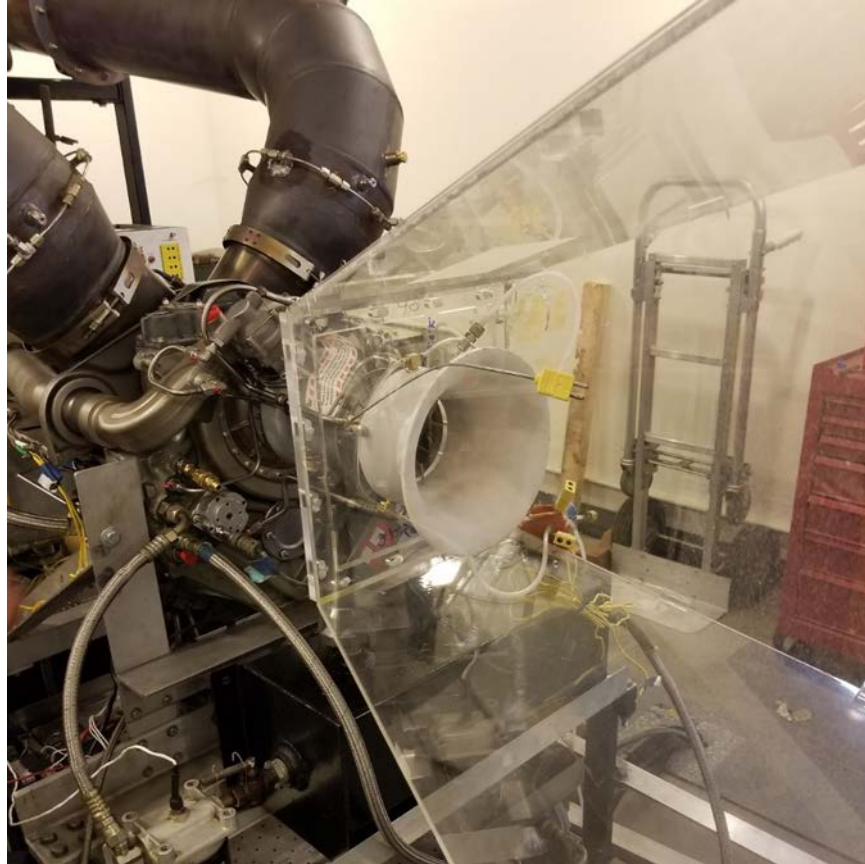


Figure 6. Bell Mouth Installed on Engine

2. Flange

The bell mouth connected to the engine and the air intake housing via a newly manufactured two part flange. This flange, made of Plexiglas, sealed the air intake for accurate monitoring. An aluminum adapter provided a smooth connection between the bell mouth and compressor of the engine. The aluminum seated in the Plexiglas, and was used because it was easier to machine to shape than a single large piece of Plexiglas, and concerns that the thin lip could crack. Importantly, the flange was recessed to accommodate a step in the compressor face, resulting in a smooth flow path to the compressor. Slots were included to ensure alignment with the engine compressor face bolt pattern and misalignment between the compressor and air intake housing (Figure 7).

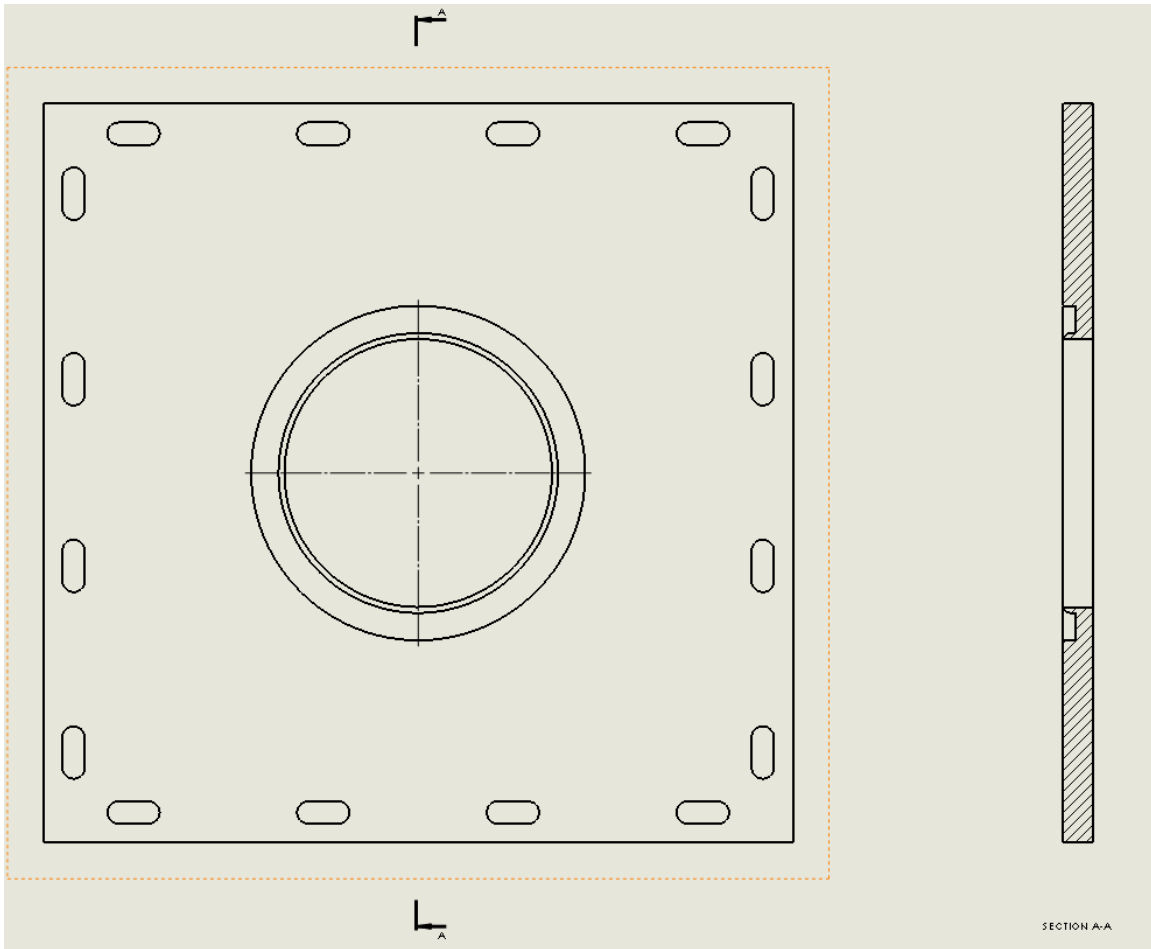


Figure 7. Flange Model Cross Section

The curved step, machined from aluminum, to the compressor mouth was fitted first by a radius gauge and second by trial and error. The iterative approach allowed for a very tight final fit that could not be obtained from measurement alone.

III. DUCT AND HEAT EXCHANGER DESIGN

A. DUCT DESIGN

The modified duct was designed using physical measurements and the thesis work done by the previous thesis student VanDenBerg [1]. VanDenBerg provided the SolidWorks model (Figure 8) of the entire exhaust duct from the engine to the exhaust nozzle. These models were confirmed by measurements and used to modify the existing infrastructure. The goal was to reuse as much of the existing ductwork as possible and the stands that supported it.

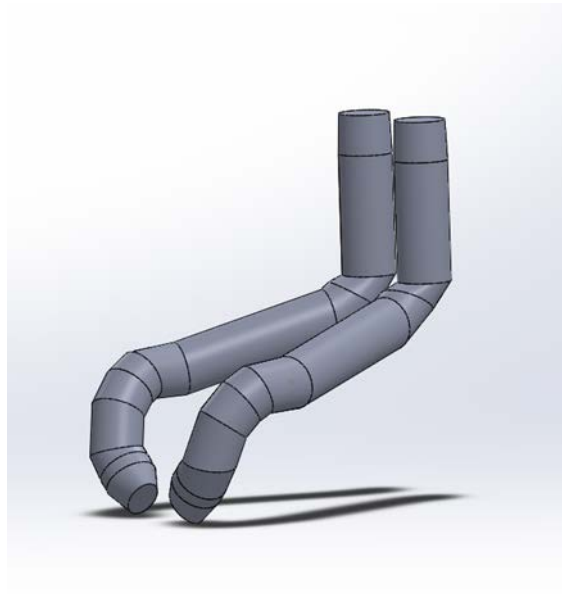


Figure 8. Exhaust Ducts by VanDenBerg. Source: [1].

The existing design space dictated the size and shape of the heat exchanger. The height to the entrance of the exhaust vent dictated the maximum height, and the separation between the two ducts dictated the maximum radius. The completed duct can be seen in Figure 9. The goal was to create a heat exchanger that did not impact engine performance despite the addition of the heat exchanger coils in the flow path. This necessitated that the duct diameter become larger. This also allowed for more tubes to be included in the design.

The maximum allowable radius was 216 mm (8.5 in.); however, a 177.8 mm (7 in.) radius was chosen to allow space between the exchangers and the possibility for future insulation around the ducting to improve performance. The final installation is shown in Figure 10.

The connection point was chosen to be the final bend in the duct. The final bend increases the diameter from 203.2 mm (8 in.) to 355.6 mm (14 in.) while not impacting available vertical height for the heat exchanger. The internal volume of the heat exchanger is a cylinder. The bend is the most complicated part to manufacture. Therefore, each bend was flattened and printed on a one-to-one scale for tracing and cutting. The bend, critically, had to match up with the existing tubing inside diameter.

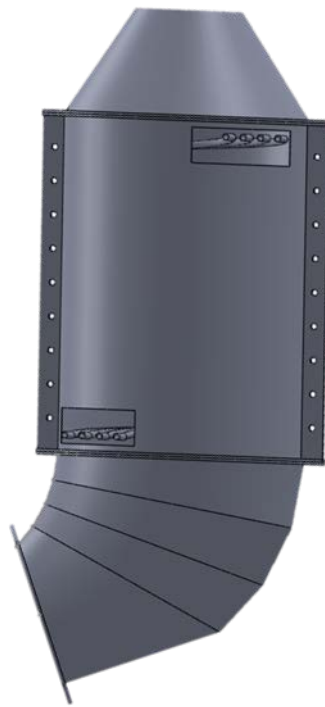


Figure 9. Assembled Model of Duct with Heat Exchanger Coils



Figure 10. Installed Heat Exchanger Duct

A nozzle was added to the top of the heat exchanger to accelerate the flow. The nozzle should be cut to match performance of the modified engine with the original duct work. The nozzle was constructed using nominal dimensions, and with the expectation that it will be made shorter during engine baseline to balance the flow between the exhaust ducts. Cutting the cone shorter will increase the flow area, decreasing the back pressure.

This is better for the engine and vitally important for accurate data measurements and repeatable experiments.

B. PRELIMINARY DESIGN CALCULATIONS

1. Heat Transfer

Vandenberg proposed a flow rate in his thesis of 0.012 kg/s CO₂. This flow rate, combined with the mass flow rate of 1.4k g/s exhaust gas (air) was used to calculate the tube length in a simple shell and tube heat exchanger. These calculations, shown in Appendix A, determined that the tube must be 1.8 m (70 in.). The length of the coils is longer than recommended, which should result in an increased mass flow rate through them. The heat exchanger used 9.525 mm (3/8 in.) tubing because it was a standard size and could be rolled with an existing roller. This tubing is well suited for the application based on size, heat tolerance, and corrosion resistance.

Table 2. Coil Length Calculations

Coil Diameter	Total Coil Length (cm)	Total Coil Length (in.)
4	239.4	94.2
6	359.1	141.4
8	478.8	188.5
10	598.5	235.6
12	718.2	282.7

2. Compressibility Limits

The heat exchanger was designed to use compressed CO₂ as the working fluid. It would be exhausted to the atmosphere after being measured. This limited the exhaust pressure to atmospheric pressure. Therefore there was an inlet pressure, which would cause the flow to choke. Choked flow would limit the mass flow rate of the system. Any pressure over the critical pressure would be irrelevant and could possibly damage the system during

testing. The critical pressure was determined using the inviscid flow approximation with the Mach number, M , equal to one in Equation 1, where P_0 is the upstream stagnation pressure, P is the downstream atmospheric pressure, γ is ratio of specific heats, which is 1.3 for CO_2 . The true critical pressure is likely less than this due to boundary layer constriction of the flow. Due to the complex and variable geometry of the inlet manifold and the tubes themselves, the analysis was not conducted for choking in the manifold.

Equation 1. Compressible Flow Pressure Relationship

$$\frac{P_0}{P} = \left(1 + \frac{\gamma - 1}{2} M^2 \right)^{\frac{\gamma}{\gamma - 1}}$$

The equation resulted in a maximum pressure of 1.832 times larger than atmospheric pressure, 185kPa. This was treated as the maximum allowable pressure in the system. In future iterations of the waste heat recovery system, the pressure may be higher, however, the pressure difference will still be constrained by the factor 1.832.

C. HEAT EXCHANGER DESIGN

Four coils were chosen as they filled the available area while retaining a significant length of coil. Equally spaced, the coils are 304.8, 254, 203.2, 152.4 mm in diameter (12, 10, 8, and 6 in.). A 101 mm (4 in.) coil could have been used, but it would have been too short to have meaningful heat transfer. These hand calculations, assuming a straight tube in tube heat exchanger were then validated by the CFD model, which showed a significant difference in the exit temperatures of the different length tubes. The hand calculations are shown in Appendix A.

The tubes were made from 9.5 mm (3/8 in.) 304 stainless steel tubing, which was selected for its size and availability. The stainless steel has good heat transfer properties, while maintaining its corrosion resistance and strength at moderately high temperatures.

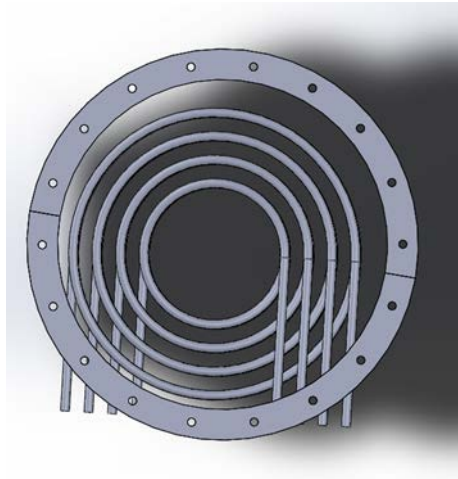


Figure 11. Axial View of Heat Exchanger

This heat exchanger will also investigate the effectiveness of helical coil heat exchangers for gas to gas applications. The helical coils have a tendency to mix the gas inside the tube leading to better overall heat transfer characteristics. The pitch was set at approximately three diameters based on the findings by Olasiman [3]. They showed that the optimal pitch; however, there was a tradeoff between flow rate and exit temperature. The coils also leave a wake of cool, slow air behind them affecting the heat transfer of the coil directly above them, reducing efficiency. The larger the gap between the coils, the more efficient the heat transfer, but this results in less overall heat in a given heat exchanger.

The heat exchanger was designed to fit within the existing test cell. This imposed limits on the overall height of the coils. The entrance and exit of the coil also needed to be 180 degrees apart to emerge on the same side of the heat exchanger. This kept the manifold centralized and away from the engine.

The final design has 431.8mm (17 in.) tall coils that revolve 7.5 times. This results in a pitch of 57.65mm (2.27 in.), or a pitch to diameter ratio of 6.05. The final design attempted to eliminate any effects the underlying tube had on the tubes above them.

D. MANIFOLD

The purpose of the manifold was to allow testing of the heat exchanger. Initially, it will be connected to a bottle of compressed CO₂ or air to the system, but has been designed with enough flexibility that it can be integrated into a larger system with minor modifications later. The second constraint is the manifold must be reconfigurable. A reconfigurable manifold allows for different flow configurations where loops are in series and in parallel. The reconfigured loop can be tested in each configuration to confirm computer models, and be used in the most efficient manner for the experimental loop designed.

The manifold, seen in Appendix B, will be attached to the CO₂ supply via 6.35mm (¼ in.) air hose. Air hose was chosen because other CO₂ supply was temporary and the inherent flexibility in tubing. It was not necessary to buy hard pipe and rout fittings to connect the bottle. Pressures are limited by the sonic limit in the tubes, which is related to atmospheric pressure. This is much less than the rated pressure of the air hose. Finally, pressure will be measured after the air hose as part of the manifold so that accurate pressure readings from the CO₂ regulator are unnecessary.

The manifold measures the inlet pressure and temperature for all tubes at one station. This reduces complexity of the data system, cost and size. It is assumed that all pressures and temperatures will be constant for all tubes. Each tube is measured individually upon exiting the heat exchanger. This gives data on each tube to confirm with the computer models. The pressure and temperature data collected by five combination probes, one inlet and four outlet, is to be recorded by the data acquisition system.

Each heat exchanger tube is connected to three of four sub-manifolds. These sub manifolds feed back into the inlet of a specific heat exchanger tube allowing a combination of tubes to flow again through the heat exchanger. In this manner, the tubes can be set in series or tubes can be paired in series, or any other combination. The use of needle valves allows throttling of each flow individually.

THIS PAGE INTENTIONALLY LEFT BLANK

IV. CFD MODELING, PREDICTIONS, AND PERFORMANCE

A. INTRODUCTION

The purpose of the computational fluid dynamics (CFD) study is to determine the effectiveness of a carbon dioxide heat exchanger located in the exhaust tubing of a T-63 turbine engine. The impact on the engine is also important to the design of the heat exchanger. The CFD models were used for design purposes, as well as for future validation of the models themselves. The validation gives confidence to future design iterations. Two models were generated for study. The first is an isothermal model used to determine the backpressure of the heat exchanger. The second model coupled the high temperature exhaust to the low temperature carbon dioxide through steel tubing. Several iterations of the heat transfer model were tested varying the boundary conditions.

B. BACKPRESSURE MOLDING

1. SolidWorks Model

The isothermal backpressure model was created in SolidWorks. A cylindrical block representing the flow volume was created and the four tubes were extrude-cut into the block. Each of these cylinders were the nominal outside diameter of 9.5 mm (3/8 in). stainless steel tubing. The final model is shown in Figure 12.

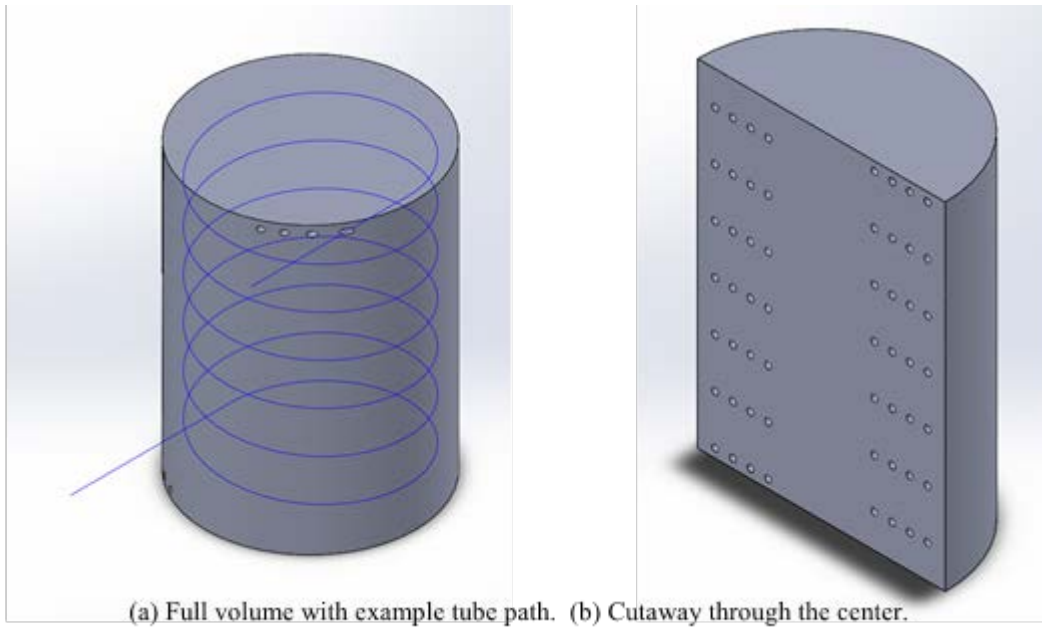


Figure 12. Flow Volume for Backpressure Model

2. Meshing

The flow volume was meshed several times. The meshing for this takes longer than normal due to the complicated internal geometry with curving helical tubes. Out of six meshes created, only two were run successfully. The others were considered either too computationally demanding or not sufficiently different from other meshes to warrant further study. The meshes that were run are summarized in Table 3.

Table 3. Backpressure Mesh Summary

	Description	Node Count	Min size	Max size
Mesh 2	Coarse mesh – no improvements	2.1M	$3.4 \times 10^{-4} \text{m}$	$6.9 \times 10^{-2} \text{m}$
Mesh 5	Medium – inflation layer 15 layers, first height $1 \times 10^{-5} \text{m}$ 1.2x growth rate	6.4M	$5 \times 10^{-4} \text{m}$	$1.5 \times 10^{-2} \text{m}$

Mesh two was designed to test the boundary conditions. It was the coarsest possible mesh, and was supposed to run as quickly as possible. It would show if the flow is developing as expected, or if changes needed to be made to the model. The full mesh can

be seen in Figure 13. Note the bands where the mesh surrounds the heat exchanger tubes and is finer, and there is no inflation layer surrounding the tubes.

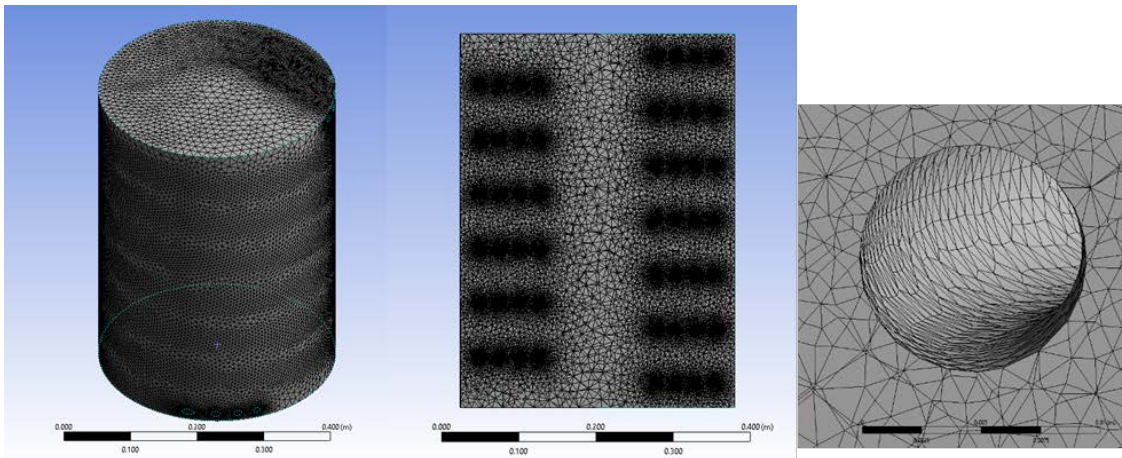


Figure 13. Backpressure Mesh 2

Mesh 5 was a refinement on mesh 2. The most important inclusion was the inflation layer. The inflation layer can be seen in Figure 14. The additional cells helped model the boundary layer accurately. Otherwise the mesh sizing was slightly reduced increasing the number of nodes. The mesh remained small to avoid long computation times.

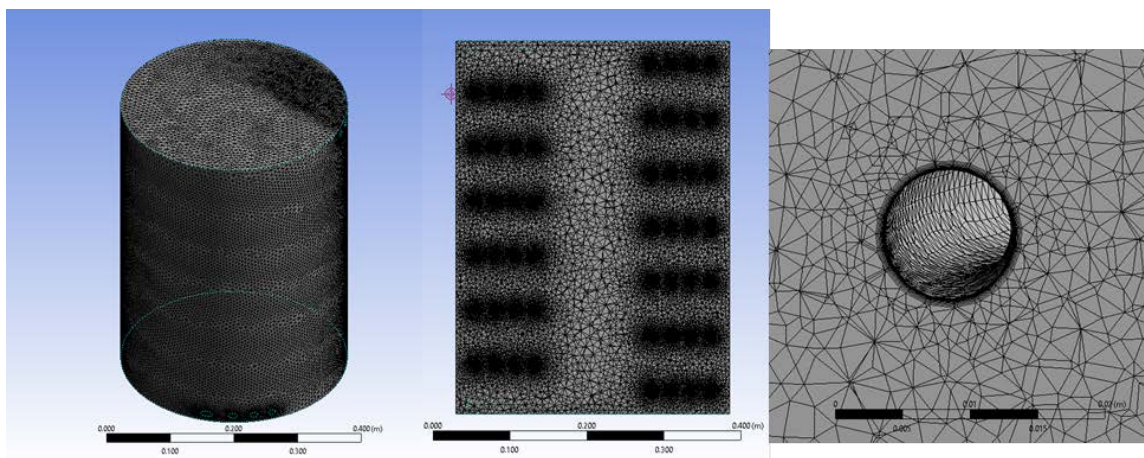


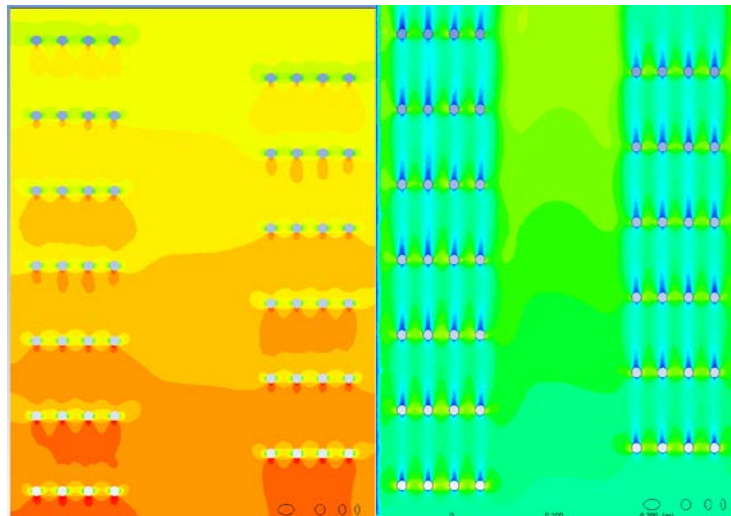
Figure 14. Backpressure Mesh 5

3. Setup

The CFD initialization was identical for both meshes. The flow moved from the bottom to the top of the cylinder. In this model the fluid is air at 400°C. This is the exhaust gasses from the engine. The inlet was a constant mass flow rate of 1.418 kg/s, the mass flow rate of the engine exhaust. The outlet was a simple opening, set to zero pressure. All other surfaces were modeled as smooth walls. This is a reasonable assumption as all ductwork and tubes will be new steel. Turbulence is modeled with the k-epsilon model due to its simplicity. The solver was set to run until the RMS value was less than 1×10^{-6} .

4. Results

The results of the fine mesh showed an average relative pressure of 139 Pa. across the inlet. Unsurprisingly, the pressure was the highest beneath the tube bundles, and lowest between the tubes themselves where the flow accelerates. This correlates well with the velocity which is fastest through the core of the heat exchanger, where there are no obstructions, see Figure 15. More precise temperature and pressure graphs at various stations throughout the heat exchanger can be seen in Appendixes C and D. Numerical results can be seen in Table 4.



Pressure distribution (left) and velocity distribution (right) for the heat exchanger

Figure 15. Backpressure Results

Table 4. Backpressure Results Summary

Run	Avg. Inlet Pressure (Pa)	Avg. Inlet Velocity (m/s)	Avg. Exit Pressure (Pa)	Avg. Exit Velocity (m/s)
5	139	12.06	.19	12.055

The most surprising result was the introduction of a large swirl in the flow, shown in Figure 16. It is believed the tube bundles themselves push the flow in the direction that they spiral. This increases the resonant time that the flow spends in the heat exchanger, increasing the heat transfer to the cool fluid. Future work can be done to increase this phenomenon, which is believed to be beneficial for the heat transfer.

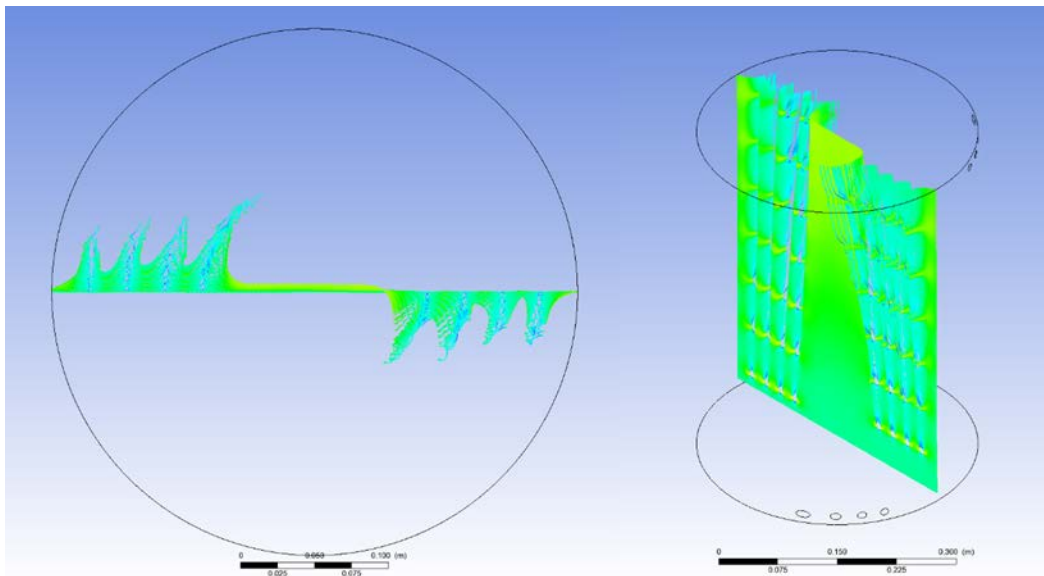


Figure 16. Swirl Induced in the Flow

C. COUPLED HEAT TRANSFER MODEL

1. Mass Flow Driven Model

a. Introduction

As with the backpressure model, the heat transfer model started in SolidWorks. In addition to the channels cut through the flow volume, four flow volumes were added for the CO₂ to flow through. They would later be thermally coupled to the exhaust. As with

the backpressure model, the first model was meshed with the coarsest mesh. This was run to test the boundary conditions and ensure that the problem could run.

b. Mesh

The mesh was refined several ways. First, the maximum face size, minimum size and the curvature normal angle were reduced. The influence can be seen in Figure 17 and Table 5. Inflation layers were added on the inside and the outside of the tubes to better capture the boundary layer effects. Externally, the creation of vortices was of interest for the heat transfer properties. Inside the tubes, the inflation layer helps capture the heat transfer from the tube wall to the carbon dioxide. The iterative mesh metrics can be seen in Table 5. All tubes used a sweep method to force cubic rather than tetragonal elements. This made the tubes more uniform and reduced the number of elements in the mesh. Unfortunately, one of the tubes would not reduce to the number of cells required, and therefore contributed approximately 1 million extra nodes to the problem. The deficiencies and detail of the final mesh can be seen in Figure 18 and Figure 19.

Table 5. Coupled Model Mesh Metrics

Mesh	Nodes (Million)	Min. element size (m)	Max. face size	Curvature normal angle	Exterior inflation (first layer thickness/ layers/ growth rate)	Interior inflation (first layer thickness/ layers/ growth rate)
1	3.5M	3.4×10^{-4}	3.5×10^{-2}	18°	N/A	N/A
3	28.5M	2×10^{-5}	2×10^{-3}	10°	2.5×10^{-5} /20/1.25	5×10^{-5} /5/1.2
4	22.0M	1×10^{-3}	2×10^{-3}	10°	2.5×10^{-5} /20/1.2	2.5×10^{-5} /5/1.2

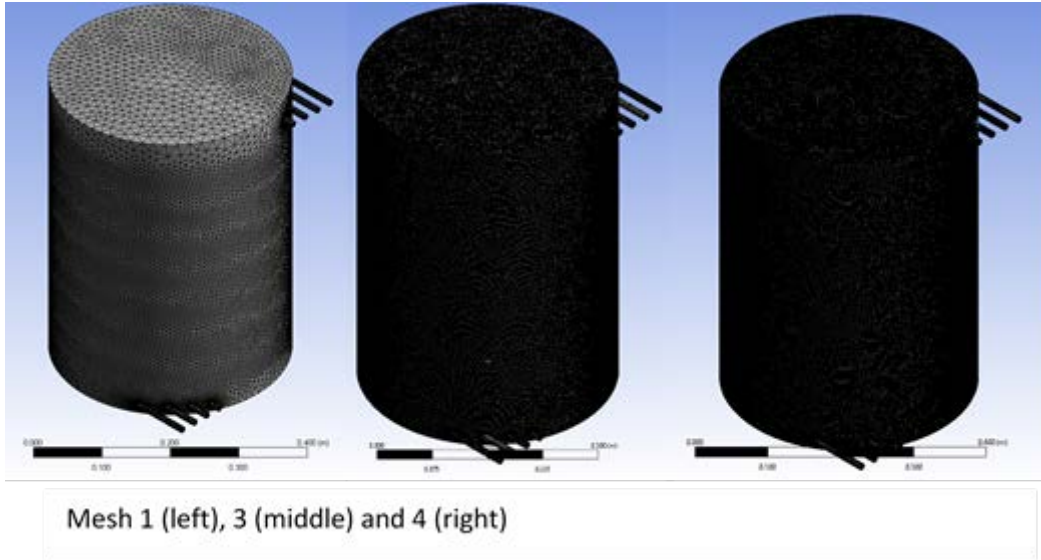


Figure 17. Mesh Overview for Coupled Mesh

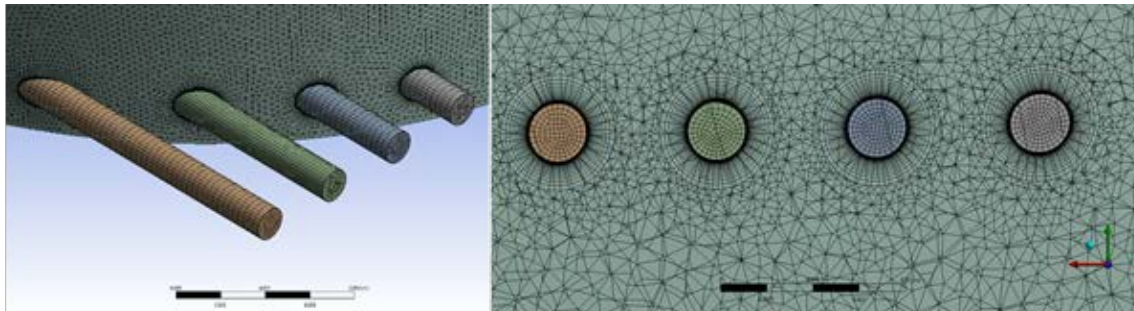


Figure 18. Detail of Mesh 4

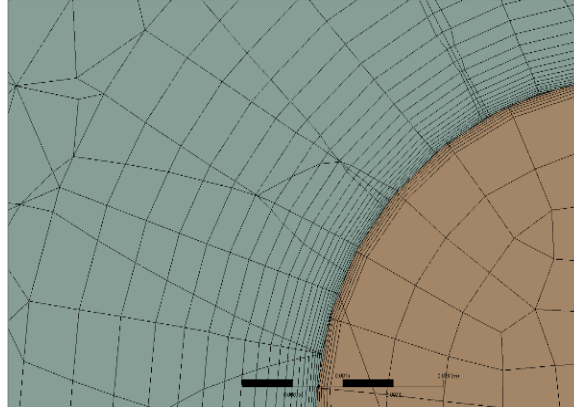


Figure 19. Detail of Mesh 4 Inflation Layer

c. Setup

The analysis for the heat exchanger was set to steady state for the initial run. The fluid in the exhaust duct was modeled as ideal air, and the tubes were modeled as ideal carbon dioxide. Each tube was considered an independent fluid volume, simulating parallel flow. The mass flow rate of each tube was set to be an equal 0.003 kg/s, and the exhaust was set at 1.418 kg/s. The tube mass flow rate came from preliminary hand calculation, and the exhaust mass flow came from prior data. The purpose of this model was to confirm the exit temperatures were reasonable given the mass flow rate, and the expected pressure loss in the tubes. The exhaust inlet was 723K and the tube inlet was set to 300K. This room temperature was chosen as it is assumed that initial testing will use ambient temperature carbon dioxide. Outlets were used for all boundaries with a static gauge pressure of 0 Pa. This simulates both the tubes and the exhaust venting to the atmosphere, which should be the initial test. A total energy model was used for the system to account for the thermal energy transfer and the slight slowdown of the fluid. The k-epsilon model for turbulence was chosen for its simplicity. A possible improvement to this model would be moving to the shear stress transport model.

The interface was defined between the tubes and the exhaust volume. The interface was defined as a thin material, with heat conduction through the wall. The wall was smooth with a transition to turbulence expected at some point. Steel was chosen as the material for the wall. The mesh connections were managed by CFX-pre through the general grid-

interface function. Therefore, the grid points along the interface did not necessarily line up, but the results were interpolated to connect the two regions.

The resulting mesh did not converge to tolerance, as Figure 20 clearly shows. There was a high-frequency instability in the flow that did not allow for convergence. Therefore, the solution was converted to a transient solution, where the total time was 0.1 seconds, with time steps every 0.001 seconds. This allowed convergence to happen, although there was still a slight wobble in the steady portion of the solution. A further study could reduce the time step again, and rerun the solution to reduce the effect of the instabilities.

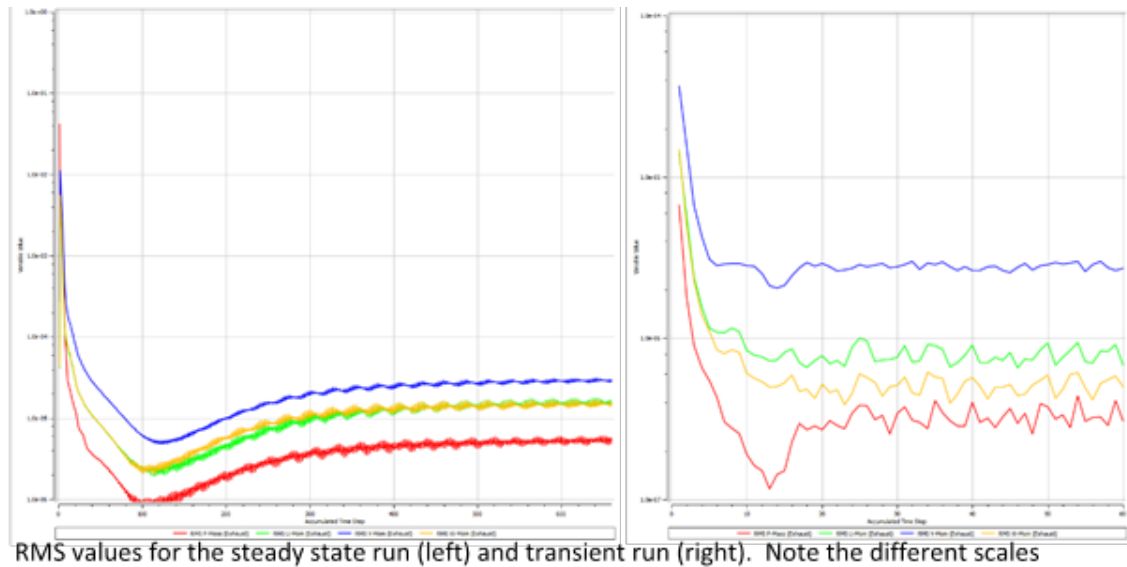
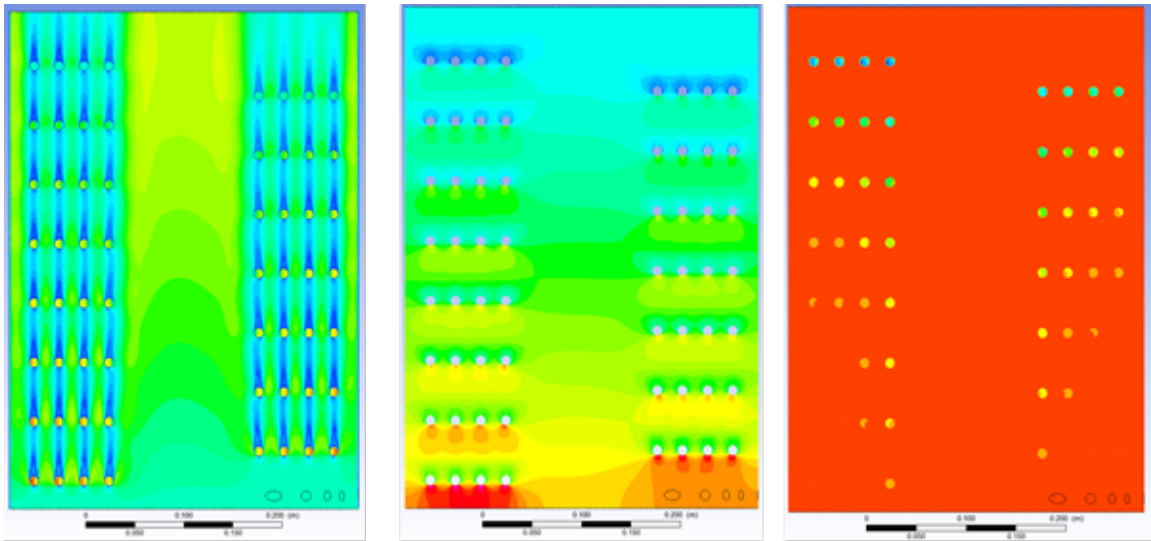


Figure 20. Heat Transfer Convergence History in Exhaust Flow

d. Results

The results of the transient run can be seen in Table 6. The varying inlet pressure are due to mass flow being specified through the tubes, allowing pressure to vary to drive the flow. Visualizations of the flow can be seen in Figure 21 and Figure 22 shows interesting patterns within the tubes. Following 25 individual velocity streamlines, the result is a logarithmic approach to the exhaust inlet temperature. There is approximately 5–40 °K temperature variation within the tube at the same height in the heat exchanger. This is most

prominent in the 152.4 mm (6 in) tube. Possible explanation is the tight radius increases the forces exerted on the fluid, separating it more, increasing the difference in temperature through the tube. The least variation is seen at the exit of the larger heat exchangers, where the fluid is nearly homogenous. The average temperature of the fluid is 693K, which could be expected if the flow is well mixed. The tube temperatures give confidence in the flow being well converged because the temperatures follow a smooth, asymptotic curve towards the maximum temperature.

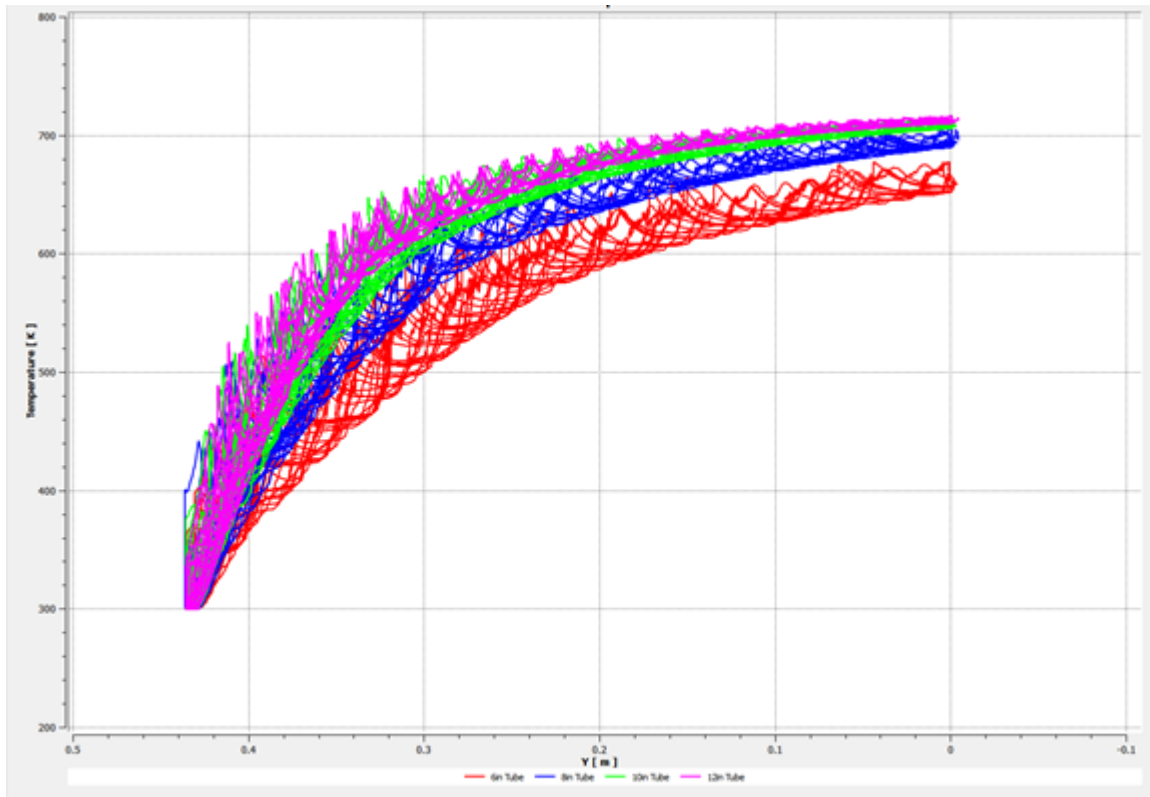


Velocity Profile (left), Pressure Profile (center) and Temperature Profile (right)

Figure 21. Mass Flow Driven CFD Results

Table 6. Mass Flow Driven Heat Transfer CFD Results

	Inlet Pressure (Pa)	Exit Pressure (Pa)	Inlet Temperature (K)	Exit Temperature (K)	Exit Velocity (m/s)
152.4 mm (6 in) tube	13,379.2	0	300	661.5	59.0
203.2 mm (8 in) tube	17,917.7	0	300	694.6	63.1
254.0 mm (10 in) tube	22,278.5	0	300	707.5	65.0
304.8 mm (12 in) tube	26,764.9	0	300	711.7	67.2
Exhaust	565.39	0	723	719.5	33.7



Streamline temperatures in the tubes. Notice the divergence even within a tube and the asymptotic behavior.

Figure 22. Mass Flow Driven Tube Temperatures

2. Steady State Pressure Driven Boundary Conditions

a. Introduction

In practice, the mass flow rate is not controlled directly. The test manifold will release a regulated pressure, resulting in the same pressure being applied to each tube. Each tube has a different friction factor, based on the length of the tube, resulting in different speeds of flow through the tube. Because each tube has the same cross section, they have different mass flow rates associated with each tube, with the shorter tubes having a faster speed and higher mass flow rate. This is the opposite of the controlled mass flow case where the pressures changed to keep the mass flow rate the same.

The pressure regulation scheme creates a problem. The shorter tubes have a higher mass flow rate and speed compared to the longer tubes. This compound problem results in generally cooler temperatures on the inner tubes.

b. Setup

The switch to pressure-driven boundary conditions also afforded the opportunity to change turbulence models. The shear stress transport model was again used, but the high speed near-wall heat transfer model was used to account for the compressibility effects near the wall. These effects should be very minor, but, the solution will be more accurate with them included. The second change was to use the blended near wall treatment. This blends the law of the wall with log law, providing a smoother boundary layer transition. For heat transfer, the boundary layer is the most important part.

The first iterations were run with static pressure at several prescribed test points to understand the correlation between pressure and mass flow. Subsequent runs focused on prescribing an inlet total pressure to closely mimic the inlet conditions present in the experimental setup. These results will be used to create a performance map of the heat exchanger.

c. Results

The results were as expected. The constant pressure condition imposed at the tube entrance resulted in varying mass flow rates through each of the tubes. The less flow resistance present in the shorter, 152.4 mm (6 in.), coil produced higher speeds and proportionally higher mass flow rates than the, larger, 304.8 mm (12 in.) coil. The slower speeds and longer resonant time in the larger coil resulted in a temperature gap between the small and large coil. Interestingly, the temperature in the small coil increased while the mass flow rate and velocity also increased. This should be investigated further due to its contradictory nature and verified experimentally. If the simulation is accurate, it means the heat transfer coefficient has increased with velocity, and it could be beneficial to increase the velocity further. It could also be an erroneous assumption on the model.

3. Pressure Driven Transient Results

Due to the instability in the exhaust flow of the steady state solution, a transient solution was attempted. The timestep was set at 0.0005 seconds to capture any vortex shedding that may have been present. This resulted in a much more stable solution, although, one that did not converge more accurately in the tubes than earlier runs.

Table 7. Transient and Steady State Comparison

Total Pressure [Pa]	Steady State Heat Transfer [w m ⁻² K ⁻¹]	Transient Heat Transfer [w m ⁻² K ⁻¹]
13.984	522.0394	522.039
20.7629	519.1762	519.1769
78.2721	489.355	489.3574
36.4039	511.8842	511.8873
57.3483	501.0414	501.0416
46.866	506.9317	??
67.8305	495.7987	495.2686

The vortices shed are important for heat transfer, as they mix the fluid. The vortices can be seen in Figure 23. The streamline, through the point marked, becomes caught in a vortex. It shows that vortices are present in the flow and can be important in the overall heat transfer of the system. Also interestingly, the streamline is carried along the top of the tube, possibly trapped between two vortices, before finally being shed and continuing up the heat exchanger. The analysis has shown the transient solutions transfer slightly more heat to the working fluid than the steady state solutions do. This comparison is shown in Table 7. There is no major difference between the heat transfer coefficients, which indicates that there is little to be gained by running a transient solution, except for vortices visualization. The full pressure study results can be seen in Appendix F.

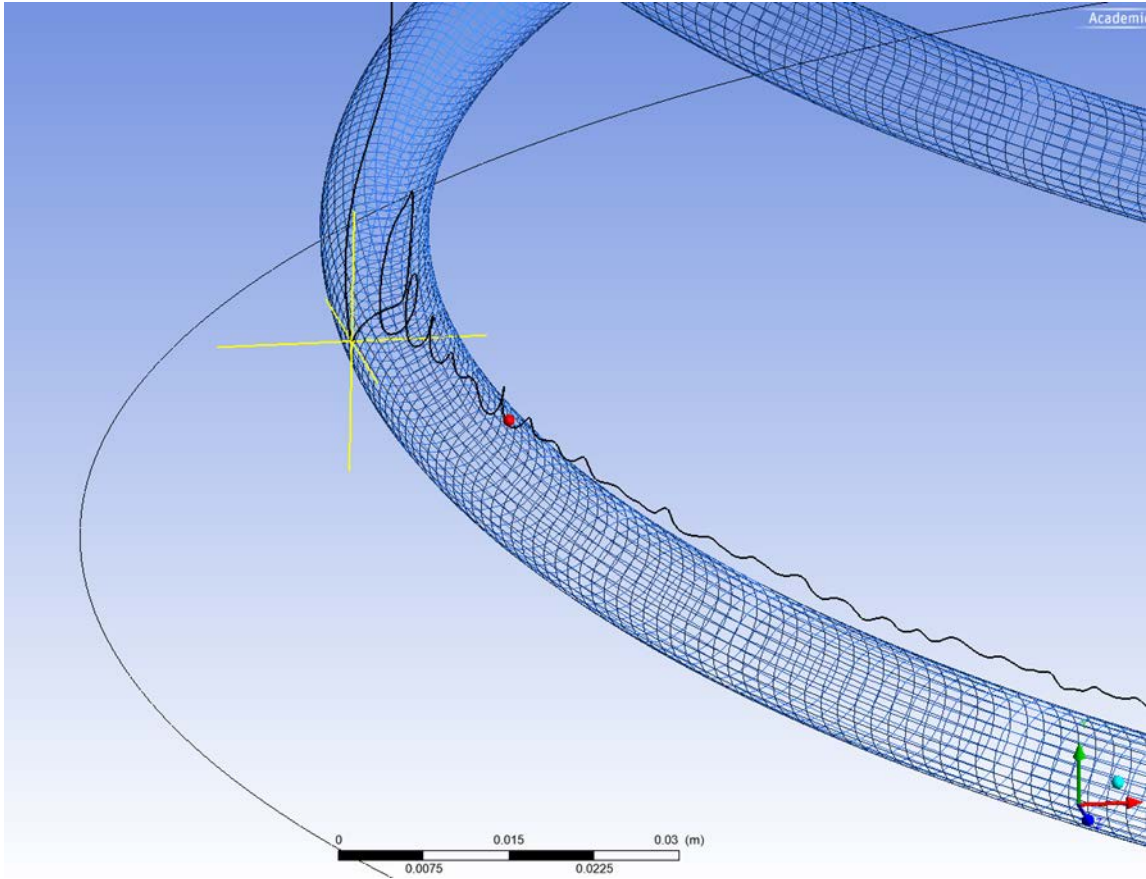


Figure 23. Streamline in a Vortex

4. Pressure Driven Transient Analytical Solution

The data from the transient solution was graphed and curve fit, Figure 24. This gives the heat transfer rate as a function of the final temperature. The final temperature is related to the mass flow rate using C_p . The C_p is allowed to vary with temperature using Equation 4 [4]. When combined, and T_i set to 300K, the resulting equation is used to relate the final temperature of the heat exchanger with the mass flow rate through the exchanger. This sets the design points for the remainder of the cycle. Finally, the mass flow rate is related to the pressure drop through the heat exchanger and will be useful for estimating performance of the cycle in the future.

Equation 2. Heat Flux Equation

$$\dot{Q} = \int_{T_i}^{T_f} \dot{m} * C_p$$

Equation 3. Heat Flux as a Function of Outlet Temperature

$$\dot{Q}(T_f) = -0.6925T_f + 840.65T_f - 243354$$

Equation 4. C_p of CO_2 [4]

$$C_p = -37357 + 30.529\theta^{0.5} - 4.1034\theta + 0.024198\theta^2$$

$$\theta = T / 100$$

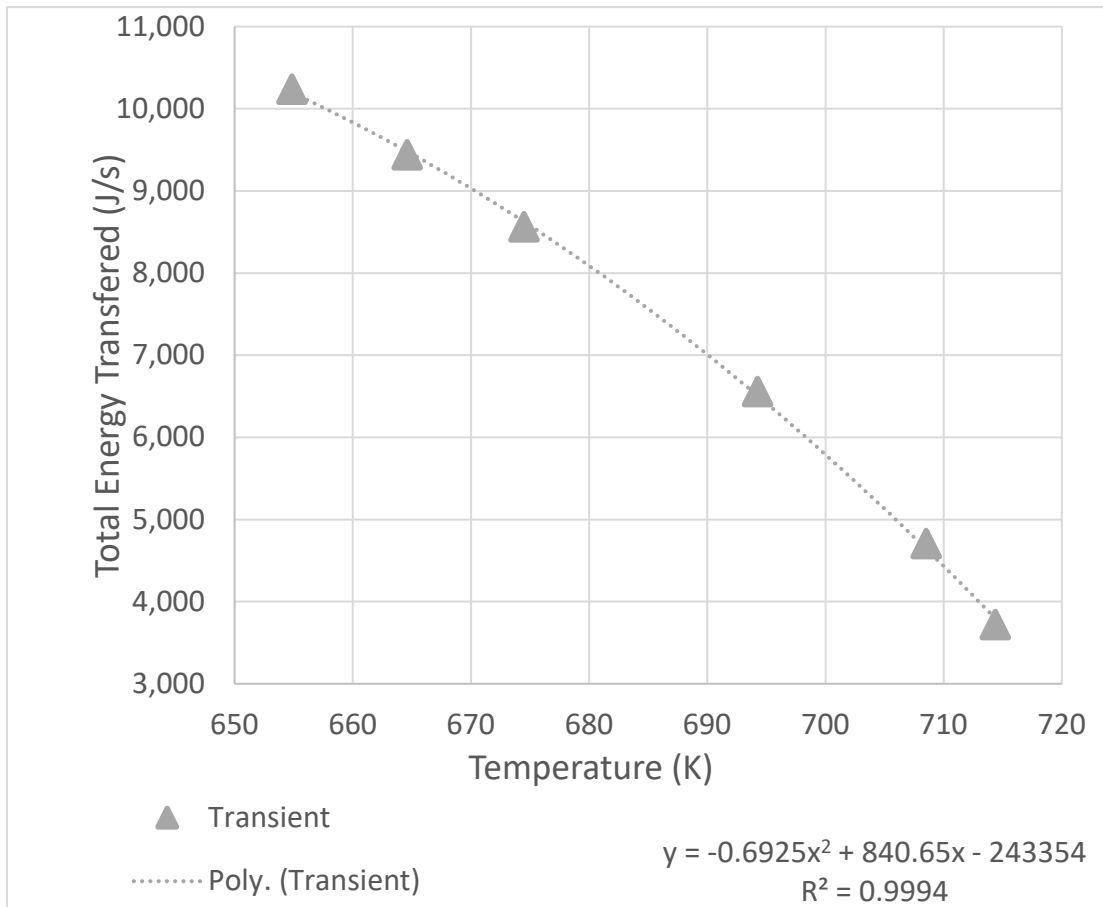


Figure 24. Transient Pressure Study Results

5. Heat Transfer and Flow Segregation

The effectiveness of the heat exchanger drops in the second half of the coils. This can be seen two places, in the temperature of the tubes and in the heat transfer coefficient of the coils. The tube temperatures can be seen in Figure 25. The tube temperatures represent 25 streamlines flowing through each tube and the temperature at each point along a stream line. Therefore, the lines taken together show the maximum and minimum temperature at any given point in the heat exchanger. The average temperature at any point is in the weighted center of the lines. The lines asymptotically approach the inlet temperature of the heat exchanger, with the distribution becoming smaller with time. The larger tube reach the equilibrium point, while the smallest tube does not. Also, most of the temperature is gained in the first half of the heat exchanger. This was corroborated by plotting the heat transfer coefficient at each point on the heat exchanger coils. This is seen in Figure 26. The exhaust flow in Figure 26 goes from the top left to the bottom right, while the flow in the coils runs counter to that. The darker the color, the smaller the heat transfer coefficient. Near the top of the heat exchanger (bottom right in the image), there is a large amount of heat transfer, and by approximately halfway through the heat exchanger, there is almost no heat transfer on the large coil. The smaller coil transfers heat through much more of the coil.

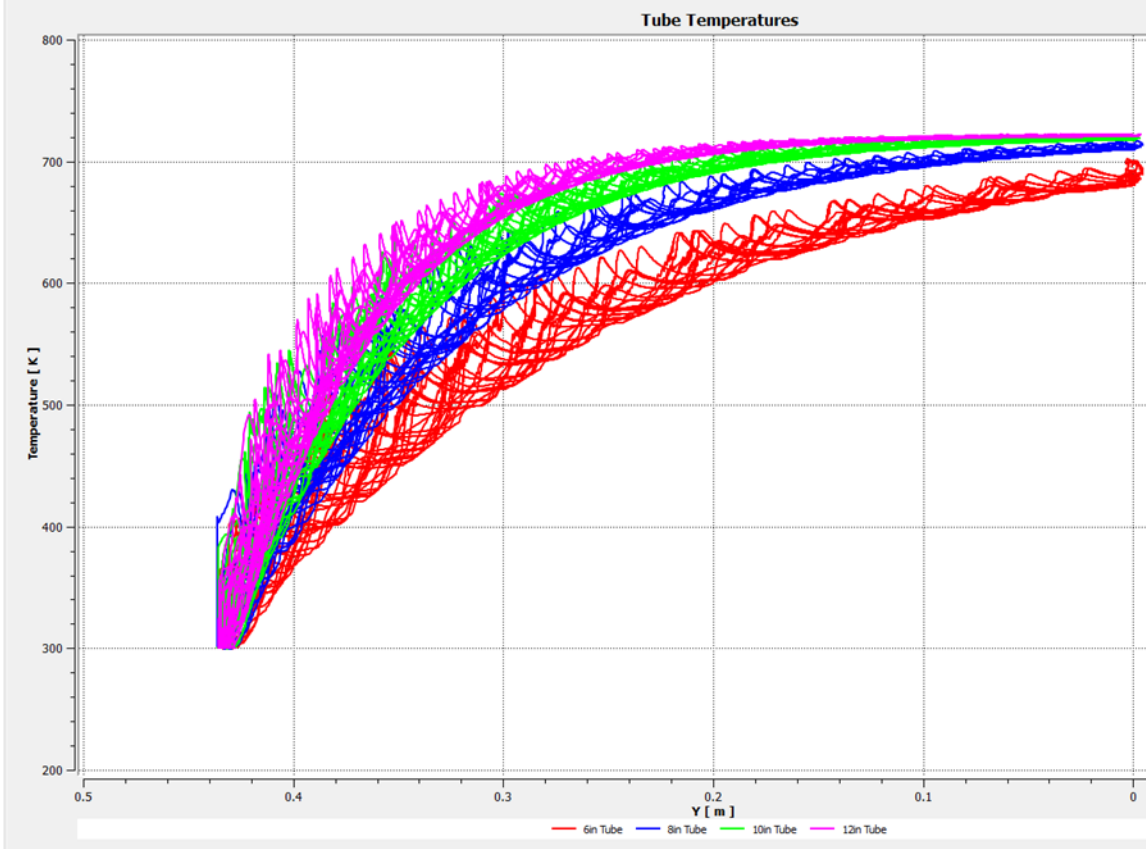


Figure 25. Tube Temperatures for Pressure Driven Boundry Conditions

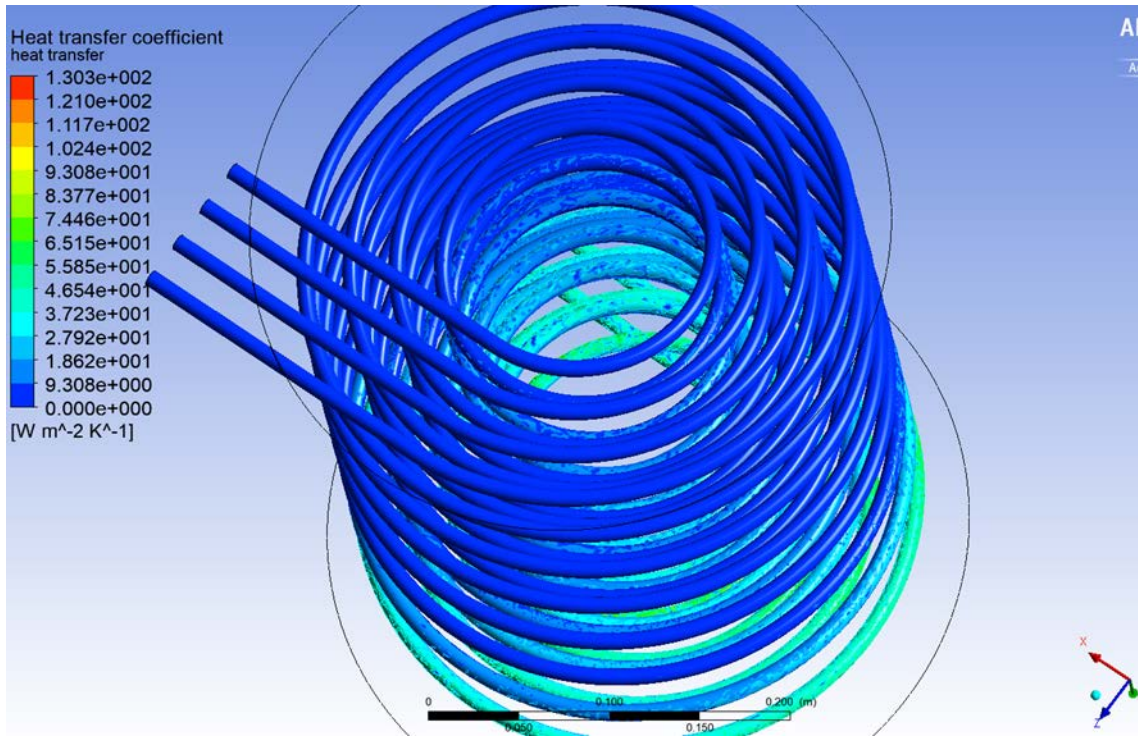


Figure 26. Heat Transfer Coefficient on Bottom of Coils

The streamline visualization, with streamlines colored for temperature instead of velocity, Figure 27, is helpful in visualizing the heat transfer through the flow. The center of the flow is very uniform and hotter than the outside of the flow. The flow that is swirling through the exchanger tubes is becoming cold, and the coldest flows are the streamlines “caught” beneath one of the tubes. This is really an issue in the top third of the exchanger; however, this top third is where most of the heat transfer occurs, and the most benefit can come from improvement. The central, hot flow channel does not mix with the swirling flow along the edges. Heat transfer could be improved by mixing some of the colder fluid with the hot fluid in the center and along the outside edge.

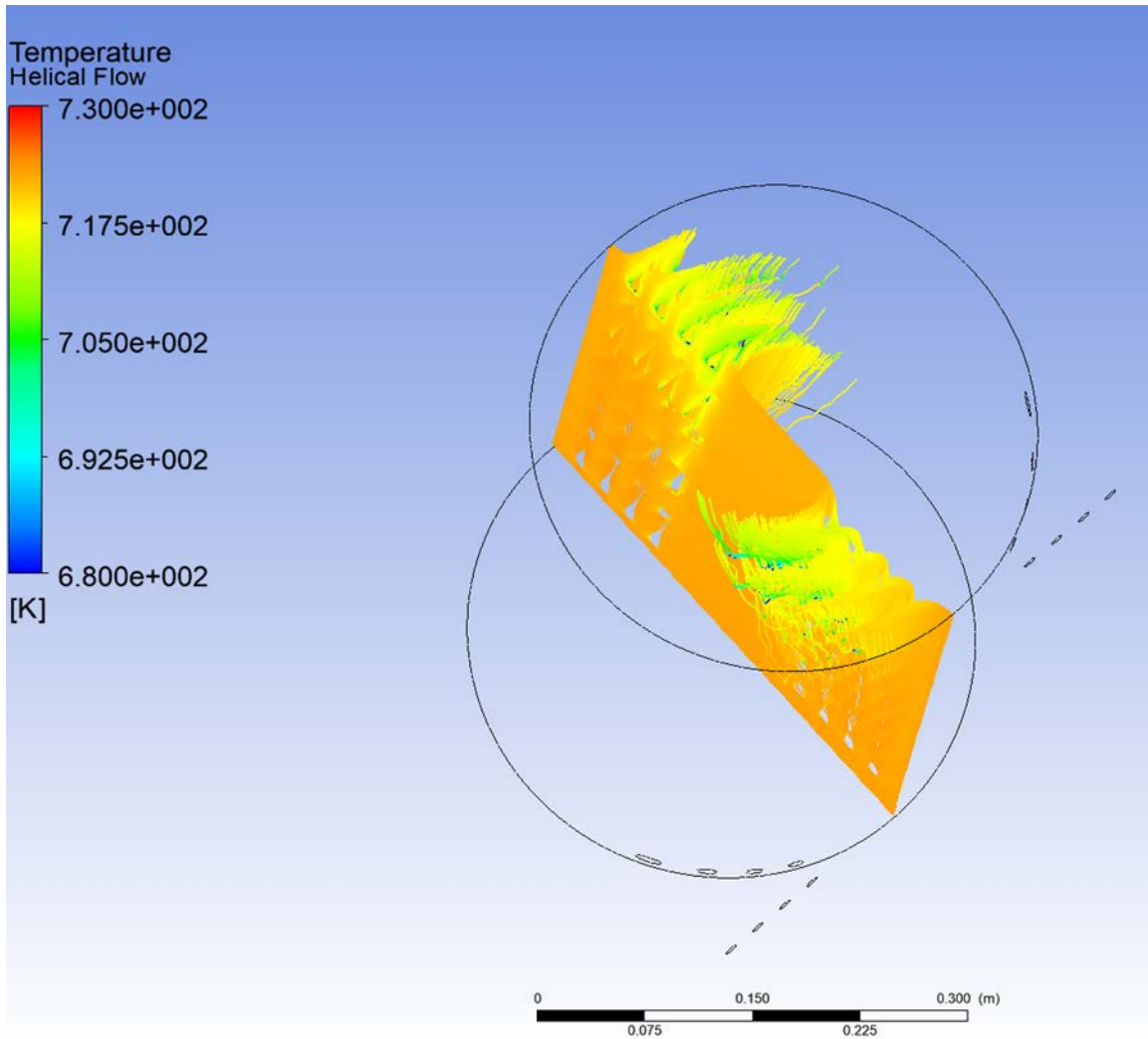


Figure 27. Streamline Visualization, Colored for Temperature

6. Mesh Independence

Mesh independence is hard to prove in this geometry because of the three-dimensional flow pattern and inherent unsteadiness of the flow. The most important aspect is accurately modeling the boundary layer. Transition is not relevant because the flow is assumed to be fully turbulent upon entering the heat exchanger. Therefore, a y^+ value of less than 10 is sufficient to resolve the boundary layer for heat transfer. A y^+ value of less than one is necessary for transition [5]; however, this simulation does not require transition modeling. The y^+ values for the tubes was approximately 3.6 for the constant mass flow rate, and 1.6 for the exterior.

THIS PAGE INTENTIONALLY LEFT BLANK

V. CONCLUSION AND RECOMMENDATIONS FOR FUTURE WORK

A. CONCLUSION

There is potential for a CO₂ waste heat recovery loop using the exhaust from the T-63 turbine engine. The proposed heat exchanger can provide the mass flow rate required in VanDenBerg's thesis to power a second Brayton cycle based on the results of CFD analysis, without impacting engine performance. The testing of the proposed heat exchanger is left to future work. There is also room for improvement in the existing design to increase the heat recovered from the heat exchanger without impacting the engine.

B. FUTURE WORK

There is much future work to be done on the heat exchanger. Design validation of both back pressure on the engine and the heat exchanger effectiveness needs to be evaluated. A more refined CFD simulation, especially a long, transient simulation, could show more detail in the bulk flow field, exposing possible improvements to the flow. The heat exchanger induces a swirl effect in the flow. This effect could be exploited by introducing small flow fins into the flow to increase the swirl throughout the heat exchanger. Several proposed methods of inducing swirl would be to add a finned center body to induce more swirl in the center of flow. A second option would be to add swirl fins along the outside of the heat exchanger. Finally, adding fins to the coils would have the effect of moving the flow and aiding in heat transfer. More tubes could be added, and if they were added by staggering them between the existing coils, the exchanger would tap energy that previously escaped. Another issue is the segregation of flow, where hot, fast flow in the exhaust duct stays separate from the cooler, swirling flow near the tubes. Mixing these two flows could increase the amount of heat transferred. A combination, which increases swirl in the beginning and mixing at the end, could be beneficial for the flow. Finally, the heat exchanger should be tested in other configurations. Parallel flow was chosen first due to its ease of modeling and testing; however, the heat exchanger could be run in a serial configuration, which might serve the final waste heat recovery loop better

than a parallel configuration. The manifold has other valve alignments that allow for a combination of parallel and serial runs. These should be investigated to see what optimization potential there could be.

APPENDIX A. HEAT EXCHANGER HAND CALCULATIONS

Engine Parameters

$$\dot{m}_{total} = 1.417 \text{ kg/s}$$

$$\dot{m}_{each} = 0.7 \text{ kg/s}$$

$$T_{hi} = 860 \text{ K}$$

$$P_{hi} = 104 \text{ kPa}$$

Fluid Parameters (air)

$$C_{p,air} = 1.1 \text{ kJ/kg-K}$$

$$\gamma_{air} = 1.33$$

$$\mu = 1.8 \times 10^{-5}$$

$$R = 287 \text{ J/kg-K}$$

$$\rho = \frac{P_{hi}}{R T_{hi}} = 0.421 \text{ kg/m}^3$$

$$\text{Pr} = 0.68$$

$$k = 5.25 \times 10^{-3} \text{ w/m-K}$$

Fluid Parameters (CO₂)

$$T_{ci} = 350 \text{ K}$$

$$T_{co} = 750 \text{ K}$$

$$C_{p,CO_2} = 850 \text{ J/kg-K}$$

$$\gamma_{CO_2} = 1.29$$

$$\mu = 1.5 \times 10^{-5} \text{ N-s/m}^2$$

$$R = 189$$

$$\text{Pr} = 0.7$$

$$k = 32.5 \times 10^{-3} \text{ w/m-K}$$

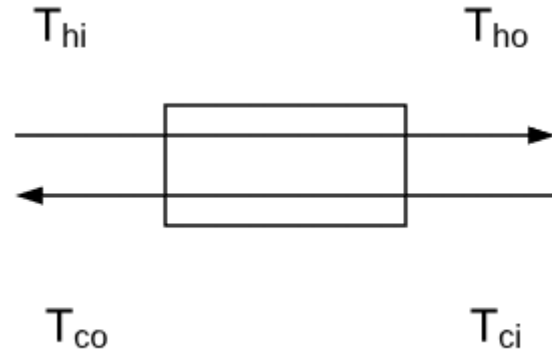
Energy Extracted from Exhaust

$$q_{out,air} = \dot{m} C_{p,air} (T_{hi} - T_{ho})$$

$$q_{out,air} = 46.3 \text{ kW}$$

$$\dot{m}_{CO_2} = \frac{q}{C_{p,CO_2} (T_{co} - T_{ci})} = 0.13 \text{ kg/s}$$

Assume 5 tubes, each 1cm in diameter



$$\dot{m}_{exhaust} = .7 / 5 = 0.14 \Rightarrow q_{exhaust} = 9.24 \text{ kW}$$

$$\dot{m}_{CO_2} = .13 / 5 = 0.027 \text{ kg/s}$$

$$Re_{CO_2} = \frac{\rho V D_{tube}}{\mu} = \frac{4 \dot{m}_{CO_2}}{\pi D_{tube} \mu} = 230,000$$

$$V_{CO_2} = 114.57 \text{ m/s}$$

$$\frac{P_{atm}}{P_{hi}} = \frac{101}{104} = 0.97$$

$$V_{exhaust} = \frac{4 \dot{m}_{each}}{\rho_{air} \pi D_{ex}} = 34.7 \text{ m/s}$$

$$Re_{exhaust} = \frac{\rho V D_{ex}}{\mu} = 198,000$$

Heat Transfer and Length Calculations

$$q = UA \Delta T_{LMTD}$$

$$\Delta T_{LMTD} = \frac{(T_{hi} - T_{co}) - (T_{ho} - T_{ci})}{\ln \left[\frac{(T_{hi} - T_{co})}{(T_{ho} - T_{ci})} \right]} = 241 \text{ K}$$

$$U = \frac{1}{\left(\frac{1}{h_i} + \frac{1}{h_o} \right)} = 675 \text{ W/m}^2 \text{ K}$$

$$Nu = 0.23 Re^{4/5} Pr^{0.4}$$

$$Nu_{air} = 0.23 Re_{air}^{4/5} Pr_{air}^{0.4} = 3405$$

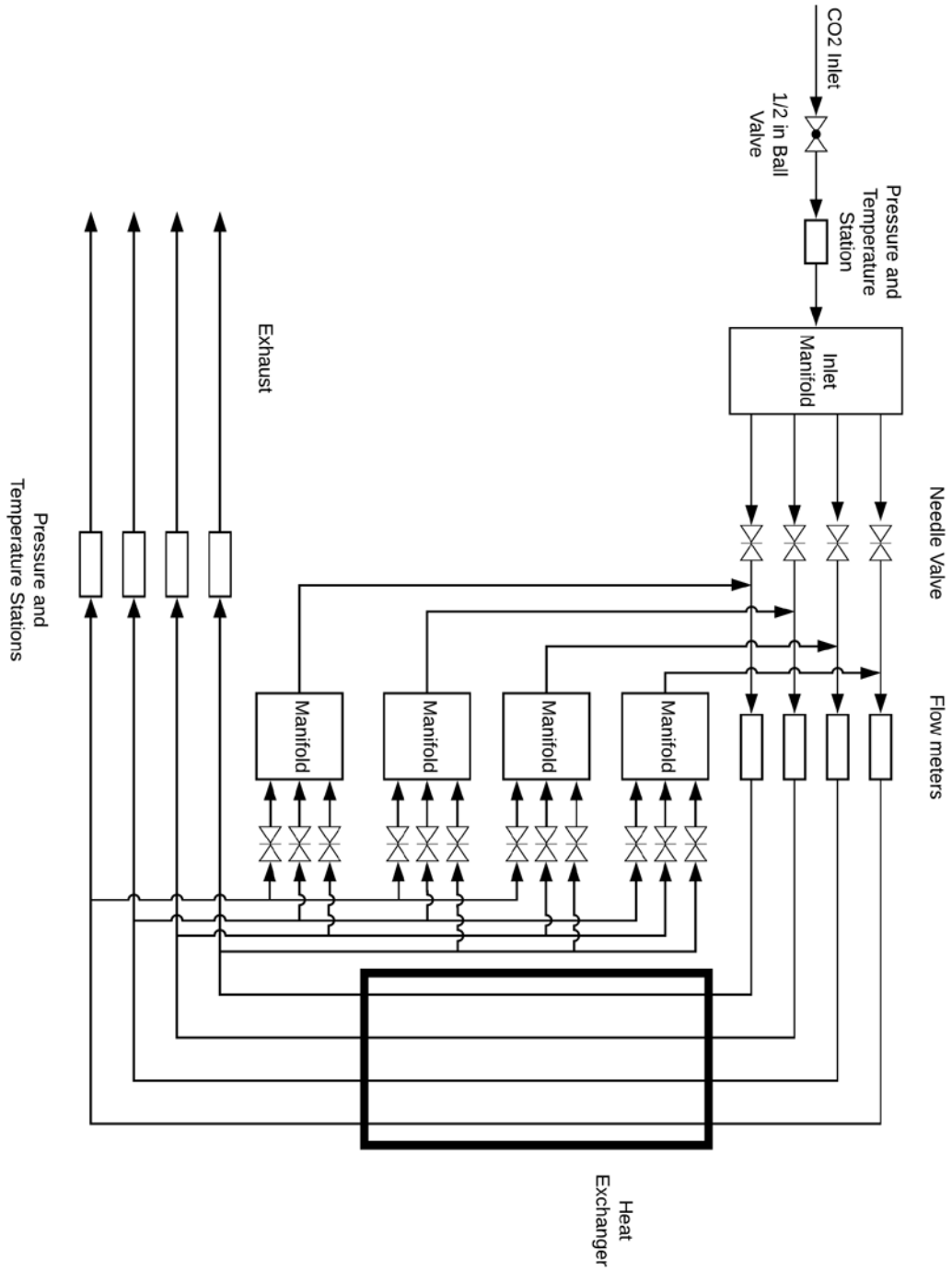
$$h_o = \frac{Nu_{air} k_{air}}{D_{ex}} = 713 \text{ W/m}^2 \text{ K}$$

$$Nu_{CO_2} = 0.23 Re_{CO_2}^{4/5} Pr_{CO_2}^{0.4} = 3937$$

$$h_i = \frac{Nu_{CO_2} k_{CO_2}}{D_{tube}} = 12797 \text{ W/m}^2 \text{ K}$$

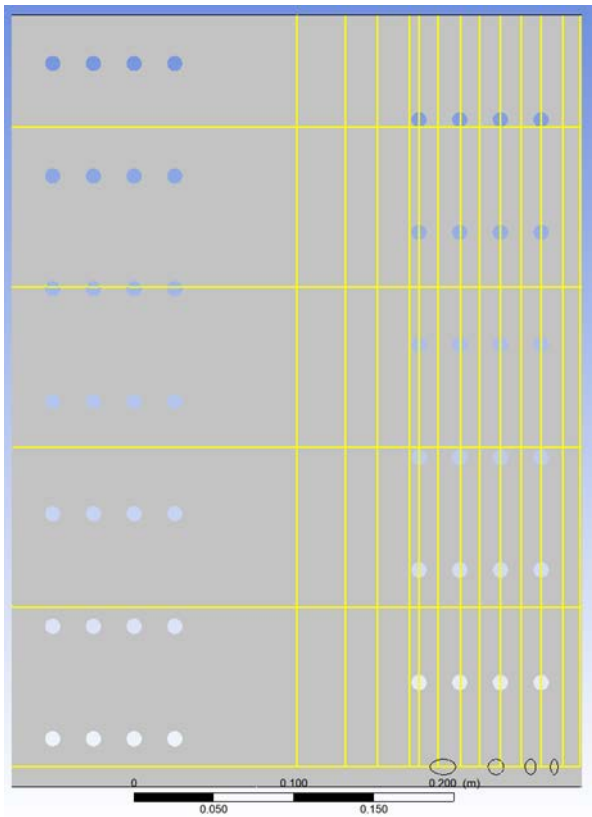
$$L_{tube} = \frac{q}{U \pi D_{tube} \Delta T_{LMTD}}$$

APPENDIX B. LINE DIAGRAM FOR MANIFOLD



THIS PAGE INTENTIONALLY LEFT BLANK

APPENDIX C. REFERENCE LINE LOCATIONS

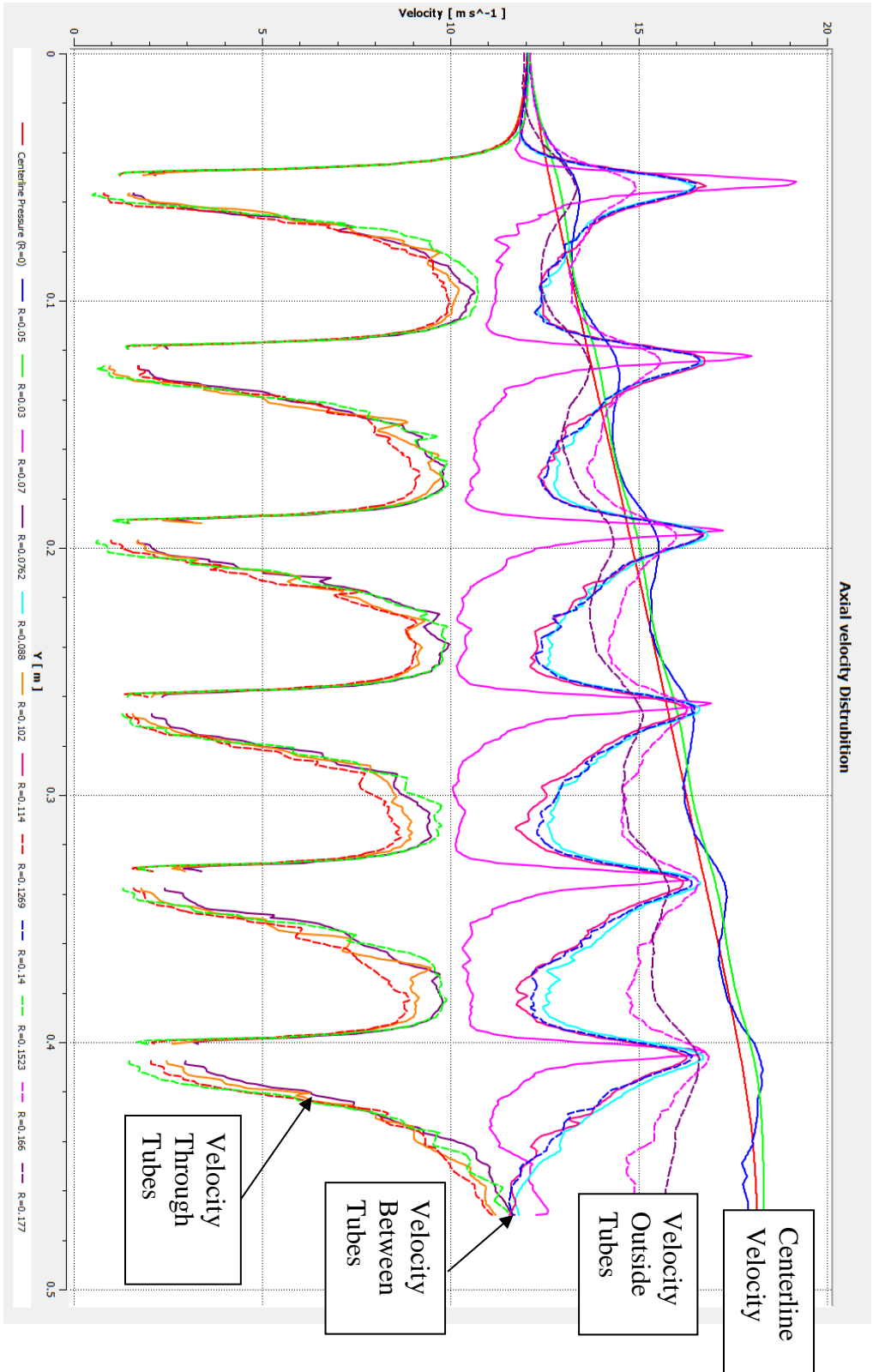


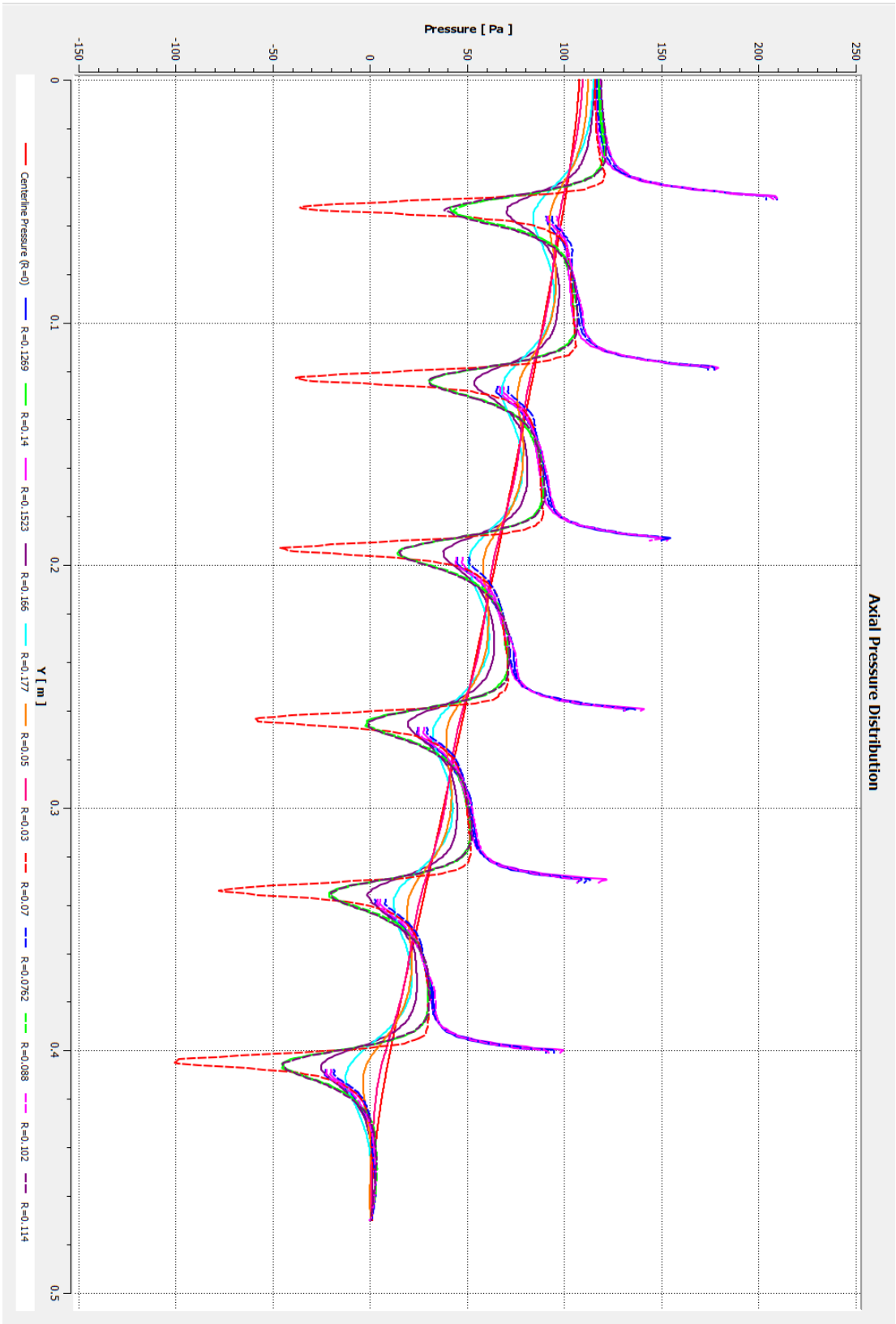
Radial Line number	Dist. From Inlet (m)
1	0.0
2	0.1
3	0.2
4	0.3
5	0.4

Axial Line number	Dist. From Center (m)	General Location
1	0.000	Centerline
2	0.030	Center Chanel
3	0.050	Center Chanel
4	0.070	Just inside 6in tube bank
5	0.076	Through 6in tube
6	0.088	Between 6in and 8in tubes
7	0.102	Through 8in tube
8	0.114	Between 8in and 10in tubes
9	0.127	Through 10in tube
10	0.140	Between 10 and 12 in tube
11	0.152	Through 12in tube
12	0.166	Between 12 in tube and wall
13	0.177	Near wall

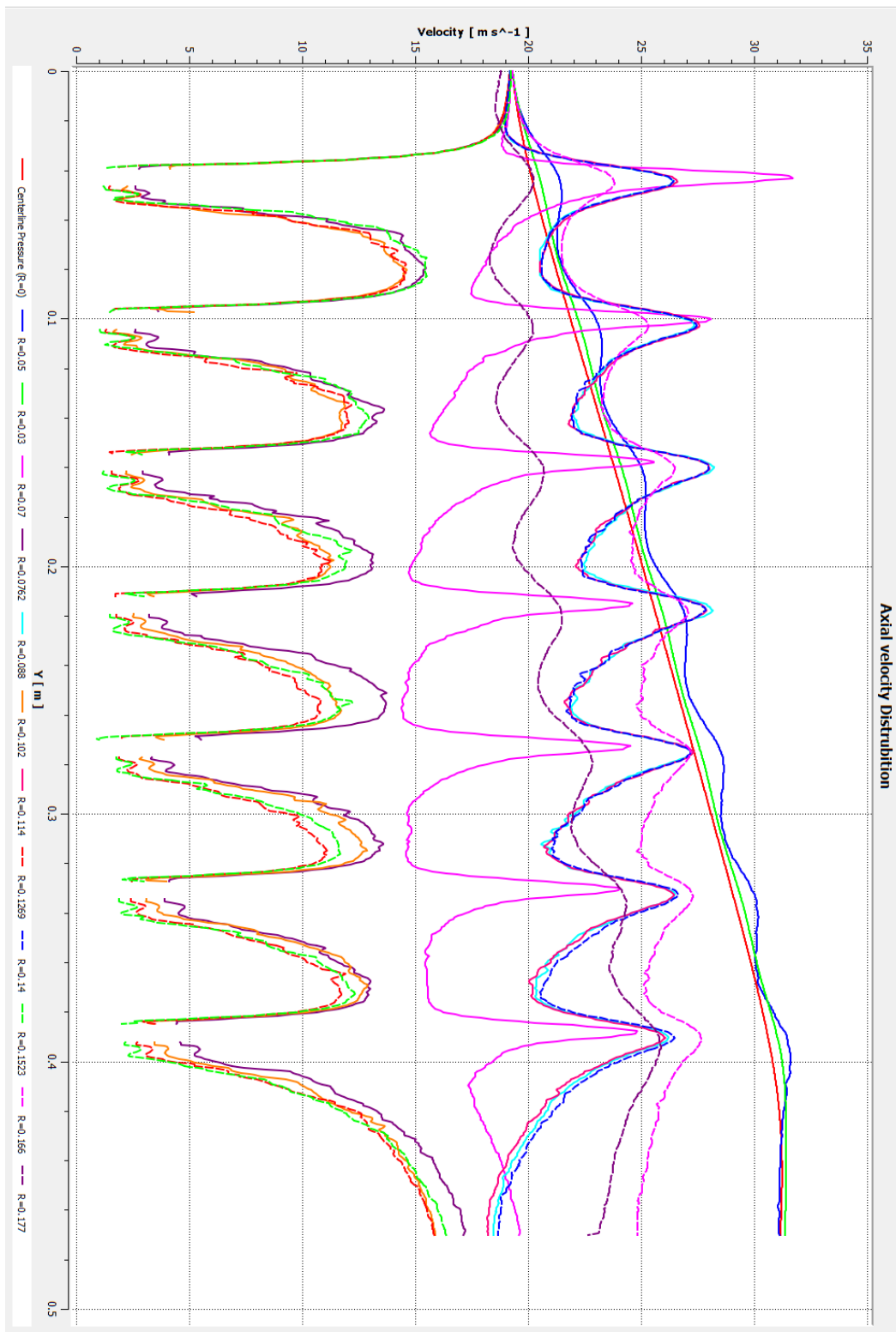
THIS PAGE INTENTIONALLY LEFT BLANK

APPENDIX D. ISOTHERMAL VELOCITY AND PRESSURE

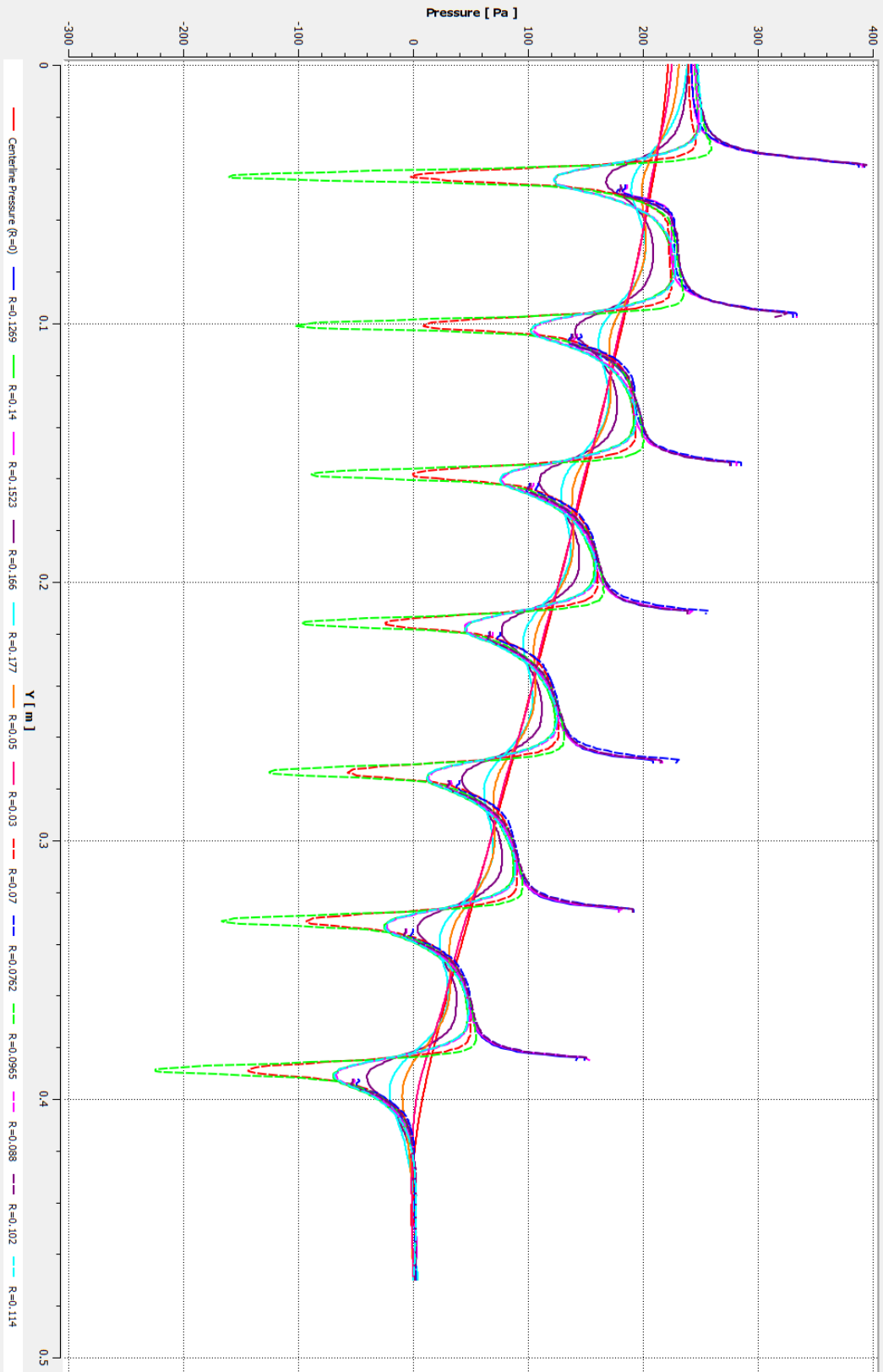




APPENDIX E. HEAT TRANSFER VELOCITY AND PRESSURE DISTRIBUTION



Axial Pressure Distribution



APPENDIX F. FULL PRESSURE STUDY RESULTS

	A	C	D	E	F
1					
2					
3	File Name	Tube Pressure Gradient (KPa)	Turbulence Model	Pressure boundary condition	Analysis Type
4	P1	13.5 static	SST	Zero Gradient	Steady
5	P1_1	13.5 static	KE	Zero Gradient	Steady
6	P1_2	13.5 static	SST	Normal To entrance	Steady
7	P2	20 Static	SST	Zero Gradient	Steady
8	P2_1	20 Static	SST	Zero Gradient	Steady
9	P3	75 Static	SST	Zero Gradient	Steady
10	P4	35 Static	SST	Zero Gradient	Steady
11	P5	55 Static	SST	Zero Gradient	Steady
12	P1T	13.5 Static	SST	Zero Gradient	Transient
14	P3T	75 Static	SST	Zero Gradient	Transient
15	P1_3	Tube Total Pres.	SST	Normal To Entrance	Steady
16	P1T_1	13.5 Static	SST	Zero Gradient	Transient
18	P3_1	Tube Total Pres.	SST	Normal To Entrance	Steady
19	P1_4	13.984 Total	SST	Normal To Entrance	Steady
20	P2_3	20.7629 Total	SST	Normal To Entrance	Steady
21	P3_2	78.2721 Total	SST	Normal To Entrance	Steady
22	P4_1	36.4039 Total	SST	Normal To Entrance	Steady
23	P5_1	57.3483 Total	SST	Normal To Entrance	Steady
24	P1_5	13.984 Total	SST	Normal To Entrance	Transient
25	P2_4	20.7629 Total	SST	Normal To Entrance	Transient
26	P3_3	78.2721 Total	SST	Normal To Entrance	Transient
27	P4_2	36.4039 Total	SST	Normal To Entrance	Transient
28	P5_2	57.3483 Total	SST	Normal To Entrance	Transient
29	P6	45 Static	SST	Zero Gradient	Steady
30	P7	65 Static	SST	Zero Gradient	Steady
31	P6_1	46.866 Total	SST	Normal To Entrance	Steady
32	P7_1	67.8305 Total	SST	Normal To Entrance	Steady
33	P6_2	46.866 Total	SST	Normal To Entrance	Transient
34	P7_2	67.8305 Total	SST	Normal To Entrance	Transient

	A	C	I
1			
2			
3	File Name	Tube Pressure Gradient (kPa)	Notes
4	P1	13.5 static	Baseline, Completed
5	P1_1	13.5 static	Unstable
6	P1_2	13.5 static	Took longer, turbulence model not as accurate
7	P2	20 Static	Wrong pressure in 8in tube
8	P2_1	20 Static	Corrected Pressure, SILN has room for improvement
9	P3	75 Static	Completed
10	P4	35 Static	4 day run
11	P5	55 Static	4 day run
12	P1T	13.5 Static	Used P1 as starting condition
14	P3T	75 Static	Used P3 as starting condition
15	P1_3	Tube Total Pres.	used P1 as a start, use tube total pressure, more realistic
16	P1T_1	13.5 Static	Time step half P1T, see if convergence is affected
18	P3_1	Tube Total Pres.	Used P3 as start, use tube total pressure, more realistic
19	P1_4	13,984 Total	7 day run, results from
20	P2_3	20,7629 Total	7 day run, results from
21	P3_2	78,2721 Total	7 day run, results from P3 and P3_1
22	P4_1	36,4039 Total	7 day run, Results from P4
23	P5_1	57,3483 Total	7 day run, Results from P5
24	P1_5	13,984 Total	7 day run, Results from P1_4, Ts=0.0005, 40 loops
25	P2_4	20,7629 Total	7 day run, using results from P2_3, Ts=0.0005, 40 loops
26	P3_3	78,2721 Total	7 day run, using results from P3_2, Ts=0.0005, 40 loops
27	P4_2	36,4039 Total	7 day run, using results from P4_1, Ts=0.0005, 40 loops
28	P5_2	57,3483 Total	7 day run, using results from P5_1, Ts=0.0005, 40 loops
29	P6	45 Static	7 day run
30	P7	65 Static	7 day run
31	P6_1	46,866 Total	7 day run, results from P6
32	P7_1	67,8305 Total	7 day run, results from P7
33	P6_2	46,866 Total	7 day run, results P6_1
34	P7_2	67,8305 Total	7 day run, Results P7_1

A	C	K	L	M	N	O	P	Q	R	
1		Results	Mass flow avg for all quantities							
2			6 inch tube							
File Name	Tube Pressure Gradient (kPa)	Velocity (m/s)	Temp (K)	Mass Flow (kg/s)	Inlet Static Enthalpy (J/kg)	Outlet Static Enthalpy (J/kg)	Heat Transfer Coefficient (J/kg-K)	Inlet Total Pressure (Pa)	Q (J)	
3	P1	13.5 static	57.15	701.84	0.002957	-44959.20	316335.00	514.7850991	13984.1	1068.347
4	P1_1	13.5 static								
5	P1_2	13.5 static								
6	P2	20 Static								
7	P2_1	20 Static	72.3153	688.814	0.00383	-44960.6	304628	507.5224952	20762.9	1339.043
8	P3	75 Static	160.342	595.623	0.00993	-44965.4	220840	446.2644995	78272.10	2639.448
9	P4	35 Static	100.382	660.775	0.005571	-44962.5	279417	490.9076463	36403.9	1807.261
10	P5	55 Static	131.479	626.677	0.007724	-44964.3	248760	468.7012608	57348.3	2268.768
11	P1T	13.5 Static	57.5197	701.675	0.002979	-44959.2	316191	514.6972601	13984.3	1075.733
12	P3T	75 Static	158.245	596.329	0.009794	-44965.6	221474	446.7996693	78338.9	2609.411
13	P1_3	Tube Total Pres.	57.6384	701.156	0.002987	-44960.3	315725	514.4151943	13981.3	1077.41
14	P1T_1	13.5 Static	57.5404	701.677	0.00298	-44959.2	316193	514.6986434	13985.1	1076.132
15	P3_1	Tube Total Pres.	158.626	595.945	0.009824	-44965.1	221129	446.5078153	78266.2	2614.058
16	P1_4	13.984 Total	57.6578	701.157	0.002988	-44960.3	315725	514.4144607	13981.2	1077.782
17	P2_3	20.7629 Total	72.4923	688.249	0.003843	-44961.8	304119	507.2013181	20759.7	1341.542
18	P3_2	78.2721 Total	158.509	595.918	0.009817	-44965.1	221105	446.4877718	78266.3	2611.992
19	P4_1	36.4039 Total	100.678	660.093	0.005594	-44963.9	278805	490.4898249	36401.4	1811.15
20	P5_1	57.3483 Total	131.908	625.873	0.00776	-44964.8	248037	468.1489695	57343.7	2273.597
21	P1_5	13.984 Total	57.658	701.156	0.002988	-44960.3	315725	514.4151943	13981.2	1077.782
22	P2_4	20.7629 Total	72.493	688.248	0.003843	-44961.8	304119	507.2020551	20759.7	1341.552
23	P3_3	78.2721 Total	158.625	595.872	0.009825	-44965.1	221063	446.4517547	78266.2	2613.723
24	P4_2	36.4039 Total	100.685	660.086	0.005594	-44963.9	278798	490.4844217	36401.4	1811.267
25	P5_2	57.3483 Total	131.911	625.872	0.00776	-44964.8	248037	468.1497175	57343.7	2273.644
26	P6	45 Static	116.781	643.153	0.006674	-44963.5	263573	479.7248866	46865.9	2059.176
27	P7	65 Static	145.597	611.009	0.008785	-44965	234673	457.6659264	67830.5	2456.578
28	P6_1	46.866 Total	116.946	642.492	0.00669	-44964.5	262980	479.2970185	46862.6	2060.3
29	P7_1	67.8305 Total	145.753	610.338	0.008804	-44965	234070	457.1811029	67824.8	2456.66
30	P6_2	46.866 Total	116.952	642.49	0.006691	-44964.5	262978	479.2953976	46862.6	2060.406
31	P7_2	67.8305 Total	145.757	610.333	0.008804	-44965	234065	457.176656	67825.8	2456.697

A	C	S	T	U	V	W	X	Y	Z
1		Results	Mass flow avg for all quantities						
2		8 inch Tube							
	Tube Pressure Gradient (KPa)	Velocity (m/s)	Temp (K)	Mass Flow (kg/s)	Inlet Static Enthalpy (J/kg)	Outlet Static Enthalpy (J/kg)	Heat Transfer Coefficient (J/kg-K)	Inlet Total Pressure (Pa)	Q (J)
3	File Name								
4	P1	13.5 static	49.3885	717.848	0.002493	-44958	330732	523.3559194	13839.1 936.4336
5	P1_1	13.5 static							
6	P1_2	13.5 static							
7	P2	20 Static							
8	P2_1	20 Static	61.4486	715.559	0.003124	-44957.1	328674	522.1527505	20223.3 1167.168
9	P3	75 Static	148.065	657.822	0.008295	-44963.7	276763	489.0786565	77522.60 2668.787
10	P4	35 Static	90.3357	699.886	0.004724	-44960.9	314582	513.7163767	36002.1 1698.657
11	P5	55 Static	120.613	680.346	0.006516	-44962.3	297014	502.6505631	56644.4 2228.331
12	P1T	13.5 Static	50.7386	717.781	0.002562	-44958.3	330672	523.3215981	13861.8 962.3198
14	P3T	75 Static	147.431	657.672	0.008261	-44963.3	276628	488.9843265	77264.4 2656.598
15	P1_3	Tube Total Pres.	50.708	717.619	0.002561	-44959.2	330526	523.2375397	13836.8 961.6026
16	P1T_1	13.5 Static	50.637	717.789	0.002557	-44958.3	330679	523.3255177	13861.1 960.3919
18	P3_1	Tube Total Pres.	147.508	658.976	0.008249	-44963.4	277801	489.796897	77517.7 2662.377
19	P1_4	13.984 Total	51.2699	717.385	0.002591	-44959.2	330316	523.1154819	13981.6 972.2367
20	P2_3	20.7629 Total	64.8913	712.519	0.003316	-44960.5	325941	520.5496274	20759.9 1229.898
21	P3_2	78.2721 Total	148.52	658.293	0.008315	-44963.4	277186	489.3708425	78267.2 2678.553
22	P4_1	36.4039 Total	91.412	699.266	0.004786	-44962.2	314025	513.3771698	36401.1 1718.066
23	P5_1	57.3483 Total	121.533	679.233	0.006577	-44963.2	296014	502.003289	57344.6 2242.655
24	P1_5	13.984 Total	51.266	717.383	0.002591	-44959.3	330314	523.1142918	13981.6 972.1642
25	P2_4	20.7629 Total	64.862	712.522	0.003314	-44960.5	325944	520.5516461	20759.9 1229.344
26	P3_3	78.2721 Total	148.422	658.336	0.008308	-44963.4	277225	489.3981189	78267.1 2676.893
27	P4_2	36.4039 Total	91.299	699.297	0.00478	-44962.3	314053	513.3945949	36401.1 1715.96
28	P5_2	57.3483 Total	121.562	679.219	0.006579	-44963.2	296001	501.9944966	57344.6 2243.159
29	P6	45 Static	106.03	690.241	0.005636	-44961.8	305910	508.3323071	46334.2 1977.496
30	P7	65 Static	134.152	669.896	0.007371	-44962.9	287618	496.4664664	66996.4 2451.344
31	P6_1	46.866 Total	106.916	689.472	0.00569	-44962.9	305219	507.8986529	46863.2 1992.549
32	P7_1	67.8305 Total	135.438	668.76	0.007455	-44963.3	286597	495.7836892	67825.9 2471.729
33	P6_2	46.866 Total	106.944	689.472	0.005692	-44962.9	305219	507.8986529	46863.2 1993.078
34	P7_2	67.8305 Total	135.373	668.784	0.007451	-44963.3	286618	495.7972978	67826.9 2470.609

A	C	AA	AB	AC	AD	AE	AF	AG	AH	
1		Results	Mass flow avg for all quantities							
2		10 inch tube								
	Tube Pressure Gradient (kPa)	Velocity (m/s)	Temp (K)	Mass Flow (kg/s)	Inlet Static Enthalpy (J/kg)	Outlet Static Enthalpy (J/kg)	Heat Transfer Coefficient (J/kg-K)	Inlet Total Pressure (Pa)	Q (J)	
3	File Name									
4	P1	13.5 static	45.524	721.303	0.00228	-44957.80	333839	525.1562797	13744.5	863.6567
5	P1_1	13.5 static								
6	P1_2	13.5 static								
7	P2	20 Static								
8	P2_1	20 Static	61.4486	719.059	0.002901	-44959.2	331821	523.99066	20435	1092.915
9	P3	75 Static	134.724	687.992	0.007201	-44964.1	303889	507.0598205	77139.4	2512.206
10	P4	35 Static	82.8618	712.55	0.004247	-44960.6	325968	520.565013	35756.6	1575.222
11	P5	55 Static	111.046	701.287	0.005807	-44962	315842	514.4883621	56227.8	2095.178
12	P1T	13.5 Static	45.419	721.264	0.002275	-44958.2	333804	525.1367045	13787	861.5893
14	P3T	75 Static	137.122	688.132	0.007328	-44963	304014	507.1367121	76720.3	2557.136
15	P1_3	Tube Total Pres.	45.4487	721.153	0.002277	-44957.6	333704	525.0780348	13743.5	862.0724
16	P1T_1	13.5 Static	45.3553	721.258	0.002272	-44958.1	333798	525.1326155	13782.1	860.3861
18	P3_1	Tube Total Pres.	135.671	687.936	0.007251	-44959.9	303838	507.0208566	77135.5	2529.245
19	P1_4	13.984 Total	46.1463	721.03	0.002313	-44957.6	333593	525.013661	13983	875.4929
20	P2_3	20.7629 Total	58.7123	718.854	0.002965	-44958.4	331636	523.8816227	20761.5	1116.73
21	P3_2	78.2721 Total	138.055	686.923	0.007391	-44960	302927	506.4424979	78268	2571.292
22	P4_1	36.4039 Total	83.253	712.197	0.004269	-44959.3	325651	520.3761038	36401.6	1582.061
23	P5_1	57.3483 Total	111.421	700.707	0.005831	-44959.7	315321	514.1674052	57344.9	2100.973
24	P1_5	13.984 Total	46.152	721.029	0.002313	-44957.6	333592	525.0130023	13983	875.6004
25	P2_4	20.7629 Total	58.716	718.854	0.002966	-44958.4	331636	523.8816227	20761.5	1116.798
26	P3_3	78.2721 Total	137.004	687.123	0.007332	-44960	303107	506.5570502	78268	2552.066
27	P4_2	36.4039 Total	83.096	712.214	0.00426	-44959.3	325666	520.3847439	36401.7	1579.042
28	P5_2	57.3483 Total	111.391	700.718	0.00583	-44959.8	315330	514.1723204	57344.9	2100.414
29	P6	45 Static	96.418	707.315	0.004989	-44961.5	321262	517.7657762	46039.6	1827.041
30	P7	65 Static	122.863	695.055	0.006491	-44962.7	310239	511.0411406	66537.2	2305.675
31	P6_1	46.866 Total	97.68	706.785	0.005059	-44959.6	320785	517.4764603	46863.2	1850.276
32	P7_1	67.8305 Total	124.694	694.066	0.006599	-44959.9	309350	510.4844496	67826.4	2337.939
33	P6_2	46.866 Total	97.604	706.789	0.005055	-44959.6	320789	517.4791911	46863.2	1848.823
34	P7_2	67.8305 Total	124.514	694.092	0.006589	-44959.9	309373	510.4984642	67827.4	2334.597

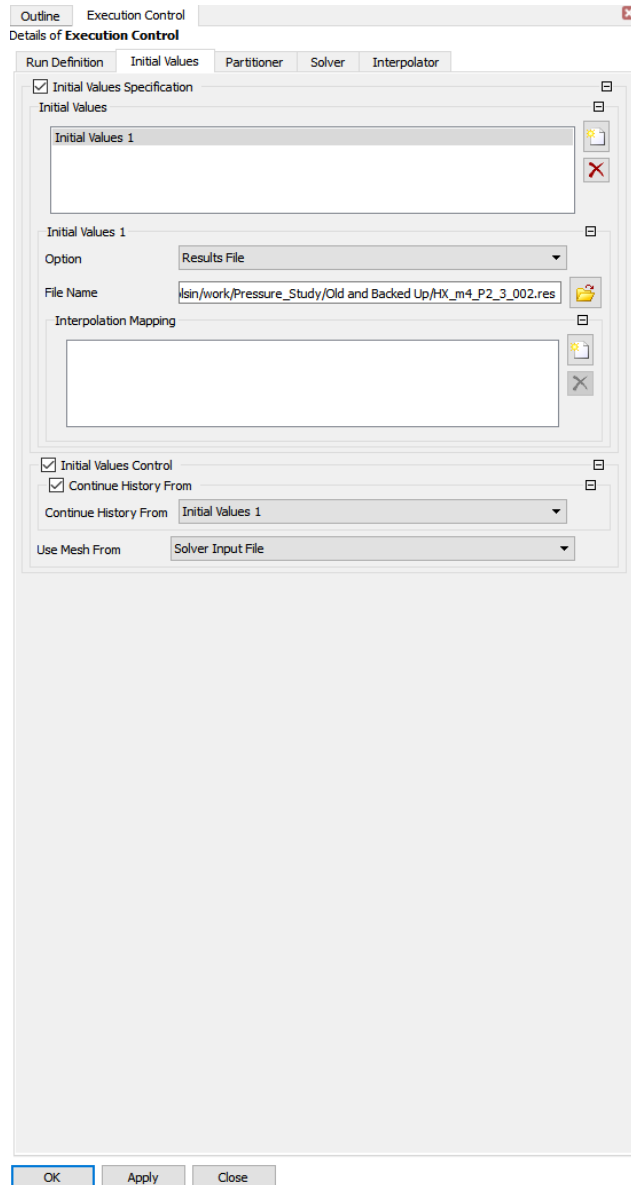
A	C	AI	AJ	AK	AL	AM	AN	AO	AP	
1		Results	Mass flow avg for all quantities							
2		12 inch tube								
	Tube Pressure Gradient (kPa)	Velocity (m/s)	Temp (K)	Mass Flow (kg/s)	Inlet Static Enthalpy (J/kg)	Outlet Static Enthalpy (J/kg)	Heat Transfer Coefficient (J/kg-K)	Inlet Total Pressure (Pa)	Q (J)	
3	File Name									
4	P1	13.5 static	36.283	722.495	0.0018	-44956.9	334910	525.7709742	13715.9	683.7604
5	P1_1	13.5 static								
6	P1_2	13.5 static								
7	P2	20 Static								
8	P2_1	20 Static	53.4291	721.215	0.002686	-44958.2	333759	525.109988	20372.2	1017.28
9	P3	75 Static	120.162	703.932	0.006268	-44961.1	318220	515.9320787	76451.9	2276.416
10	P4	35 Static	75.2297	717.904	0.003823	-44959	330783	523.3875281	35592.3	1436.484
11	P5	55 Static	101.928	711.386	0.005252	-44960.3	324922	519.9459928	56038.3	1942.733
12	P1T	13.5 Static	41.1988	722.225	0.002058	-44957.3	334668	525.6330091	13735.3	781.2385
14	P3T	75 Static	124.377	702.98	0.006502	-44960.90	317362.00	515.4121685	76401.1	2355.845
15	P1_3	Tube Total Pres.	41.4584	722.241	0.002071	-44958.1	334682	525.6418564	13714.3	786.1018
16	P1T_1	13.5 Static	41.1634	722.215	0.002056	-44957.3	334658	525.6264409	13735.3	780.5498
18	P3_1	Tube Total Pres.	124.378	703.455	0.006498	-44961.5	317791	515.6726443	76448.6	2357.057
19	P1_4	13.984 Total	41.9782	722.188	0.002098	-44958.1	334634	525.6139676	13982.1	796.3197
20	P2_3	20.7629 Total	53.6386	721.139	0.002698	-44959.1	333691	525.0722815	20760.3	1021.651
21	P3_2	78.2721 Total	125.4	702.439	0.006561	-44961.5	316878	515.1187505	78268.2	2373.928
22	P4_1	36.4039 Total	76.154	717.722	0.003872	-44960.5	330619	523.293838	36400.7	1454.364
23	P5_1	57.3483 Total	102.353	711.194	0.005275	-44961.3	324750	519.8459211	57345.2	1950.26
24	P1_5	13.984 Total	41.969	722.187	0.002097	-44958.2	334633	525.6134491	13982.1	796.1508
25	P2_4	20.7629 Total	53.628	721.139	0.002698	-44959.1	333691	525.0722815	20760.3	1021.447
26	P3_3	78.2721 Total	126.602	702.265	0.006627	-44961.5	316721	515.022819	78268.6	2396.725
27	P4_2	36.4039 Total	76.069	717.707	0.003868	-44960.5	330605	523.2852682	36400.8	1452.661
28	P5_2	57.3483 Total	102.296	711.202	0.005272	-44961.3	324757	519.8499161	57345.2	1949.181
29	P6	45 Static	88.242	715.08	0.004514	-44959.9	328243	521.9037031	45863.8	1684.47
30	P7	65 Static	112.746	707.789	0.005846	-44960.8	321689	518.0213312	66263.9	2143.548
31	P6_1	46.866 Total	89.618	714.735	0.004587	-44961	327933	521.723436	46863	1710.51
32	P7_1	67.8305 Total	114.881	707.053	0.005965	-44961.5	321027	517.62527	67827	2183.034
33	P6_2	46.866 Total	89.513	714.739	0.004582	-44961	327937	521.7261126	46863	1708.492
34	P7_2	67.8305 Total	114.657	707.066	0.005953	-44961.5	321038	517.6313102	67828	2178.729

A	C	AQ	AR	AS	AT	AU	AV	AW	
1		Results	Mass flow avg for all quantities						
2									
3	File Name	Tube Pressure Gradient (kPa)	Total mass flow (kg/s)	Mass Flow Average Temp (K)	Avg Heat Transfer Coefficient t	Q Total (J/s)	Average Total Pressure (Pa)	Maximum Total Pressure (Pa)	Backpressure (Pa)
4	P1	13.5 static	0.00953	714.5836	522.2671	3552.197697	13820.9	13984.1	545.19
5	P1_1	13.5 static							
6	P1_2	13.5 static							
7	P2	20 Static							
8	P2_1	20 Static	0.012541	709.4114	519.694	4616.405578	20448.4	20762.9	544.26
9	P3	75 Static	0.031695	654.3086	489.5838	10096.85674	77346.5	78272.1	537.26
10	P4	35 Static	0.018366	694.7002	512.1441	6517.624453	35938.7	36403.9	
11	P5	55 Static	0.025299	675.211	501.4465	8535.009673	56564.7	57348.3	539.587
12	P1T	13.5 Static	0.009873	714.6508	522.1971	3680.880385	13842.1	13984.3	545.027
14	P3T	75 Static	0.031884	655.0689	489.5832	10178.9902	77181.2	78338.9	537.30
15	P1_3	Tube Total Pres.	0.009895	714.4295	522.0932	3687.1870	13819.0	13981.3	545.068
16	P1T_1	13.5 Static	0.009864	714.6434	522.1958	3677.4603	13840.9	13985.1	545.019
18	P3_1	Tube Total Pres.	0.031822	655.1988	489.7496	10162.7370	77342.0	78266.2	537.411
19	P1_4	13.984 Total	0.009989	714.3833	522.0394	3721.8311	13982.0	13983.0	
20	P2_3	20.7629 Total	0.012823	708.5238	519.1762	4709.8216	20760.4	20761.5	543.953
21	P3_2	78.2721 Total	0.032083	654.8304	489.355	10235.7642	78267.4	78268.2	537.304
22	P4_1	36.4039 Total	0.018521	694.2736	511.8842	6565.6416	36401.2	36401.6	
23	P5_1	57.3483 Total	0.025443	674.5075	501.0414	8567.4857	57344.6	57345.2	539.439
24	P1_5	13.984 Total	0.009989	714.3818	522.039	3721.6972	13982.0	13983.0	545.039
25	P2_4	20.7629 Total	0.012821	708.5234	519.1769	4709.1416	20760.4	20761.5	
26	P3_3	78.2721 Total	0.032092	654.8604	489.3574	10239.4069	78267.5	78268.6	537.264
27	P4_2	36.4039 Total	0.018502	694.264	511.8873	6558.9296	36401.3	36401.7	541.805
28	P5_2	57.3483 Total	0.025441	674.5016	501.0416	8566.3979	57344.6	57345.2	539.393
29	P6	45 Static	0.021812	684.8783	506.9317	7548.1830	46275.9	46865.9	540.716
30	P7	65 Static	0.028493	665.2469	495.7987	9357.1450	66907.0	67830.5	538.474
31	P6_1	46.866 Total	0.022027	684.4395	506.5989	7613.6345	46863.0	46863.2	
32	P7_1	67.8305 Total	0.028822	664.6325	495.2686	9449.3616	67826.0	67827.0	
33	P6_2	46.866 Total	0.022019	684.4286	506.5998	7610.7986	46863.0	46863.2	
34	P7_2	67.8305 Total	0.028797	664.6171	495.2759	9440.6321	67827.0	67828.0	538.298

THIS PAGE INTENTIONALLY LEFT BLANK

APPENDIX G. RESTARTING A RUN ON HAMMING

Control for runs on the Hamming cluster must be done before writing the .def file for the restart. Initial values for the file can be specified under execution control/Initial values. Checking the box allows the addition of .res files from which the solver will pull initial conditions. This is helpful when runs have to be restarted, small changes in boundary conditions, or a new mesh is used.



Checking Initial Values Control/Continue History From continues the solver run from where the initial values left off. Again, a new mesh can be chosen. Write the .def file and the .sh file as normal, and run the batch file. The solver will show a continued history.

THIS PAGE INTENTIONALLY LEFT BLANK

LIST OF REFERENCES

- [1] VanDenBerg, A., “Energy Efficient Waste Heat Recovery From an Engine Exhaust System.” Master’s thesis. Naval Postgraduate School, Monterey, CA. 2016. <http://hdl.handle.net/10945/51630>
- [2] Moran, M., *Fundamentals of Engineering Thermodynamics*, John Wiley and Sons, Hoboken, NJ, USA: (2014).
- [3] Olasiman, L A M., “Optimization of Helical Coil Heat Exchanger as a Waste Recovery System for Fuel Consumption.” *Research & Review: Journal of Engineering Technology*, Vol. 5, No. 3 (2016): pp. 57–61. <http://www.rroj.com/open-access/optimization-of-helical-coil-heat-exchanger-as-a-waste-recoverysystem-for-efficient-fuel-consumption-.php?aid=83799>.
- [4] Hill, P., and Peterson, C., *Mechanics and Thermodynamics of Propulsion*, Addison-Wesley Publishing Company, 1992.
- [5] SAS IP, INC., “SHARCNET CFX-Solver Theory Guide,” [Online]. Available: https://www.sharcnet.ca/Software/Ansys/17.0/en-us/help/cfx_thry/cfx_thry.html. [Accessed 30 5 2018].

THIS PAGE INTENTIONALLY LEFT BLANK

INITIAL DISTRIBUTION LIST

1. Defense Technical Information Center
Ft. Belvoir, Virginia
2. Dudley Knox Library
Naval Postgraduate School
Monterey, California